CHAPTER 3

Pile/Soil Interaction Model & Dynamic Signal Analysis

1. Introduction

The main topic of this research is the analysis of dynamic data. As it was explained in chapter 1, this kind of analysis is not as simple as the static load test analysis. Since the measurements are influenced by the inertial efforts and obviously by the loading rate, and since the data are generally measured with transducers requiring a pre-treatment before exploitation, the method used to analyse these data is complex and requires to assess the pile/soil interaction system.

This chapter is focused on the presentation of this model and on the analysis of the dynamic data. The pile and soil are described in simple elements and defined by their mechanical or geomechanical parameters. The pile/soil model is described in term of fundamental relationships for both static and dynamic fields and for both base and shaft specific resistances. The algorithms used to perform the analysis of the dynamic signals and to simulate the static load-settlement curve are presented and the parameters required to describe this system are classified and sorted with respect to their reliability.

Since the model specificity is the possibility to account for the loading rate effect through the generation of viscous and radiation terms added to the static soil reaction, it is also helpful to define, to introduce and to illustrate each term involved in the process and to explain the way to evaluate the total rheologic stress. This fundamental approach is the practical continuation of the theoretical presentation of the loading rate effect in chapter 2.

After, a complete analysis of the dynamic data is proposed because their evolutions are typical of the loading rate. This analysis includes the study of the sole quantities measured (force, velocity, as well as derived settlement and energy) and an overview of the signal quality with a special aspect to the post-treatment performed.

2. Presentation of the model

This section is focused on the description of the general pile/soil model. The main algorithm of resolution, the pile, the shaft and base reactions and the back-analysis program are described, commented and justified as needed.

2.1. Pile model description

The pile and its environment are modelled by a lumped mass model as described on Figure III-1. This system allows the discretization of the dynamic (force) and the kinetic (acceleration, velocity and displacement) fields for both pile and soil elements directly adjacent at the pile interface.

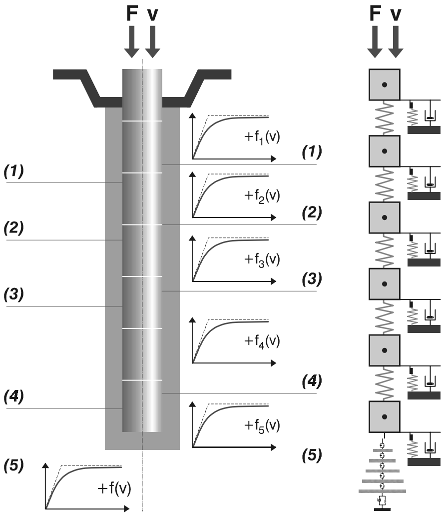

Figure III-1 : General description of the model NUMSUM-UCL

The system is defined by the stiffness, dampings, masses and dimensions of each component and some of them are either unknown or known. The model receives input data (force, velocity, displacement signals) and generates the pile/soil response (stress and deformation) in agreement with the pile/soil interaction definition. The number of unknowns is relatively large and function of the discretization. A good knowledge of the pile/soil environment (mechanical, geotechnical, geometrical) is required to reduce the number of unknowns to an acceptable and manageable amount. The pile/soil interaction is based on a modelling of the soil behaviour by two approaches: the shaft and base reactions. These models are developed by Holeyman (1984, 1985 & 1988) and described in chapter 2 and here below.

The pile is composed of lumped elements (springs and masses). The measured signals are imposed on the pile head. The integration scheme is explicit: the system state at time t is known and used to evaluate the system state at time t + Δt. The stability and the convergence of the system, in particular, depend on the relation between the mechanical characteristics of each element and the set time increment.

At each time step, for each node of the system, the balance of forces is evaluated (Equ. III- 1). These forces are the internal forces of the pile coming from the upper and lower node displacements (due to the input signal imposed in the pile head), and the external forces coming from the soil reaction (shaft friction for the nodes inside the pile and shaft friction and base resistance for the lower pile element). This force balance allows the evaluation of the acceleration of the concerned element (application of Newton's first law - Equ. III- 2), and by simple and double integration, its velocity and displacement respectively (Equ. III- 3 to Equ. III- 5). This motion description allows the calculation of the stress state for each element by means of the chosen stress-displacement and the defined velocity dependent relationships. Consecutively, the balance of forces is re-evaluated and the cycle loops until the end of the calculation duration.

The nodes are located at the centre of the masses and a corresponding stiffness is evaluated from the pile material. This process is summarized on Figure III-2 and the following equations:

$$F_{result,i}(t) = \sum F_{\text{int},i}(t) + \sum F_{ext,i}(t)$$ **Equ. III- 1**

$$acc_i(t) = \frac{F_{result,i}(t)}{mass_i}$$ **Equ. III- 2**

$$vel_i(t + \Delta t) = vel_i(t) + acc_i(t) \cdot \Delta t$$ **Equ. III- 3**

$$\Delta displ_i(t) = vel_i(t + \Delta t) \cdot \Delta t$$ **Equ. III- 4**

$$displ_i(t + \Delta t) = displ_i(i,t) + \Delta displ_i(t)$$ **Equ. III- 5**

- $F_{result,\,i}(t)$ is the resulting force at the node i at the time t;

- $F_{int,\,i}(t)$ is one of the internal forces applied at the node i at the time t;

- $F_{ext,\,i}(t)$ is one of the external forces applied at the node i at the time t;

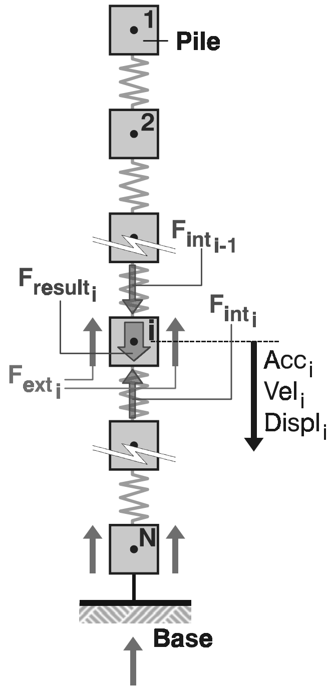

Figure III-2 : Model description

- $Mass_i$ is the mass of the element i;

- Acc_i, Vel_i, $\Delta displ_i$ and $displ_i(t)$ are the acceleration, the velocity, the increment of displacement and the displacement of the node i at time t, respectively;

– Δt is the time increment.

The system must be initiated with one field (force, acceleration, velocity or displacement) varying in time (a pulse, a dirac, a constant increase, or decrease,…). The system resolution also requires the calculation of the internal and external forces in function of the pile motion. This calculation is ruled by constitutive laws described hereafter.

In this model, only the pile is moving. The soil is supposed motionless and the reaction is located at the interface between the pile and the soil. The pile motion is consequently considered as the relative motion between pile and soil.

2.2. Pile/soil interaction model

2.2.1 Pile model

2.2.1.1 Stiffness

The pile is considered as an elastic material with an elastic modulus E_p and divided in N elements of equal lengths [1 to N]. Each element is limited in dimensions, so its mass and stiffness can be calculated.

$$mass_i = \rho_p \cdot A_i \cdot h_i$$ **Equ. III- 6**

- ρ_p is the volumetric mass or mass density of the pile material [kg/m³];
- A_i is the normal section of the element i supposed to remain constant along the element and in time [m²];
- h_i is the height of the element, generally set to $\frac{H_p}{N}$ [m].

$$k_{el,i} = \frac{E_p . A_i}{h_i}$$ **Equ. III- 7**

This is the elementary stiffness of the pile element. However, the spring used in the model is located in a mid position between two lumped masses (Figure III-2). The used equivalent stiffness is given by:

$$k_{calc,i} = \frac{1}{\frac{1}{\frac{k_{el,i-1}}{2}} + \frac{1}{\frac{k_{el,i}}{2}}} = 2 \cdot \frac{k_{el,i-1} \cdot .k_{el,i}}{k_{el,i-1} + k_{el,i}}$$ **Equ. III- 8**

Where $k_{el,i}$ and $k_{el,i-1}$ are the elementary stiffness of two consecutive pile elements.

2.2.1.2 Internal forces

The internal forces are calculated taking into account the transmitted forces coming from the head pile or the base and the resulting shortenings of the pile elements. Spring forces are purely elastic:

$$F_{\text{int},i} = k_{calc,i} \cdot (displ_{i-1} - displ_i)$$ **Equ. III- 9**

A small damping behaviour is introduced to account for all energy losses:

$$F_{\text{int},i} = k_{calc,i} \cdot (displ_{i-1} - displ_i) + C_p \cdot I \cdot (vel_{i-1} - vel_i)$$ **Equ. III- 10**

- C_p is the damping factor (0.5) [-];
- I is the nominal impedance of the pile [MPa.s/m];

2.2.2 Shaft model

The lateral shaft friction is composed of a static and a dynamic term. Each component is described with its own relationships between soil resistance and either displacement or velocity. The shaft model does not take into account the potential interactions between the soil layers.

2.2.2.1 Elastic and plastic deformations in the static field

Stress-strain relationship (τ,γ)

The stress-strain relationships is described by elasto-plastic and hyperbolic laws (Figure III-3):

Elasto-plastic

$$\tau = G_i \cdot \gamma \rightarrow \gamma \le \gamma_r$$

$$\tau = \tau_{ult} \rightarrow \gamma \ge \gamma_r \quad \textbf{Equ. III- 11}$$

- τ is the shear stress [Pa];
- G_i is the initial shear modulus [Pa];
- γ is the angular distortion [-].

Hyperbolic

$$\gamma = \gamma_r \frac{\eta}{1-\eta} \quad \textbf{Equ. III- 12}$$

- γ_r is the reference shear strain: $\frac{\tau_{ult}}{G_i}$ [-];
- η is the mobilization ratio: $\frac{\tau}{\tau_{ult}}$ [-];
- τ_{ult} is the ultimate shear stress [Pa].

The change from linear elasticity to a constant strength in plasticity does not reflect the reality.

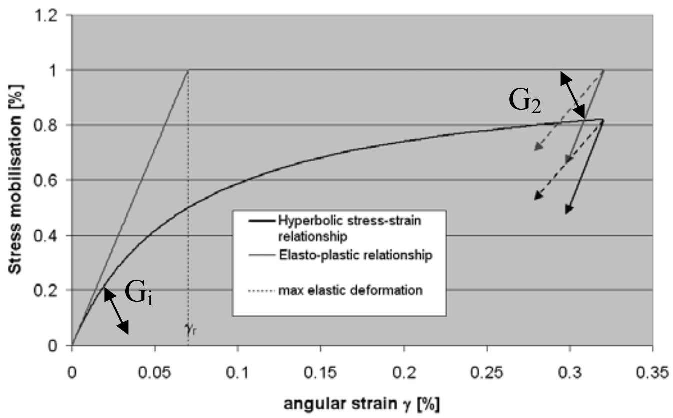

Figure III-3 : τ–γ relationship proposed for the shaft reaction

A smooth formulation may be established in order to progressively introduce plasticity. Kondner (1963) proposes the hyperbolic law (Equ. III-12), where the stress tends asymptotically to the ultimate shear stress τ_{ult} with increasing deformation. This relationship smoothly indicates the transition between linear to non-linear behaviours and respects the elastic behaviour in case of small strains, and the plastic deformation in case of large strains.

The unloading phase follows a linear path characterised by the initial shear modulus G_i or a different modulus given by the ratio: $\frac{G_i}{G_2}$ (Figure III-3).

Stress-displacement relationship (τ,displ)

The stress-displacement relation for the shaft is obtained after integration of the angular distortion of the soil. This integration must be performed on a finite domain in order to give a finite displacement:

$$displ_p = \frac{\tau_p \cdot R_p}{G_i}\int_{R_p}^{\infty}\frac{dr}{r} = \frac{\tau_{pile} \cdot R_p}{G_i}\ln(r)\Big|_{R_p}^{r=\infty} = \infty$$ **Equ. III- 13**

- R_p is the pile radius [m];
- τ_p is the stress mobilized at the pile shaft [Pa].

Randolph & Wroth (1978) suggest the decomposition of the soil behaviour in a half space accounting for the base resistance and a layer of depth D accounting for the friction. They also reduce the infinite layer to a finite space with an outer boundary. This limit is fixed to a distance, called R_m, where the soil vertical stress induced by the vertical displacement of the pile is considered as negligible:

$$R_m = 2.5D \cdot (1-\upsilon)$$ **Equ. III- 14**

- D is the embedded pile length or the soil layer thickness [m];
- υ is the Poisson ratio [-].

Using this boundary, Equ. III- 13 becomes:

$$displ_p = \frac{\tau_p \cdot R_p}{G_i}\int_{R_p}^{R_m}\frac{dr}{r} = \frac{\tau_p \cdot R_p}{G_i}\ln\left(\frac{R_m}{R_p}\right) = \frac{\tau_p \cdot R_p}{G_i}\cdot\ln(\frac{R_m}{R_p})$$ **Equ. III- 15**

That is the stress-displacement relationship at the pile shaft for an elasto-plastic law.

If the hyperbolic law proposed by Kondner (1963) is used, the same process gives:

$$displ_p = \int_{R_p}^{R_{m1}}\gamma \cdot dr = \frac{\tau_p R_p}{G_i}\ln\left(\frac{\frac{R_m}{R_p}-\eta_p}{1-\eta_p}\right)$$ **Equ. III- 16**

- τ_p, $displ_p$ is the pile shaft stress-displacement state;
- η_p is the mobilization ratio at pile shaft ($\frac{\tau_p}{\tau_{ult}}$).

This approach allows also the direct introduction of the hysteretic damping by the introduction of a completely elastic unloading phase respecting the stiffness of the elastic spring (with a possible factor accounting for the modification of the shear modulus for the unloading : $G_i \rightarrow G_2$).

The static term, for both elastic or plastic deformations is completely described with three parameters:

- The ultimate shear resistance τ_{ult};
- The initial shear modulus G_i;
- Poisson's ratio υ.

It can be modelled by a non linear spring with a plastic slider in case of the use of an elasto-plastic relationship (Figure III-4).

2.2.2.2 Elastic and plastic deformations under dynamic solicitations

The shaft model acts under dynamic solicitations with two terms linked to the loading rate:

- A viscous damping supposed to represent the dissipative energy lost at the interface;
- A radiation damping supposed to represent the energy lost in the surrounding soil.

The sum of all terms (static + viscous + radiation) is limited to a velocity dependent term.

The viscous damping

As observed by numerous researches (see chapter 2), there is an increase of soil resistance due to an increasing loading rate. This term is velocity dependent following a non-linear relationship (a power law) and proportional to the static soil reaction:

$$\tau_{visq} = J.v^N.\tau_{stat}$$ **Equ. III- 17**

τ_{visq} is the viscous stress [Pa]; N s the exponent expressing the non-linear dependency [-];

v is the pile velocity [m/s]; J is the damping factor [s/m^N].

τ_{stat} is the static soil reaction [Pa];

The law has an empirical origin and its parameters, J and N are based on the literature. N is generally set to 0.2 and J is function of the site, pile and soil types.

The radiation damping

The radiation damping is introduced in chapter 2, based on Novak et al.'s work (1978). That work concerned the analysis of the harmonic vibration of an infinite and rigid cylinder in an infinite medium. A complex stiffness of the medium has been found to represent the soil response. The imaginary part of this expression model the radiation of the energy into the soil and is simplified by the following expression for high frequencies:

$$c = \frac{G_i}{V_s} = \sqrt{\rho \cdot G_i} \text{ [Pa.s/m]}$$ **Equ. III- 18**

Where ρ is the volumetric mass of the soil [kg/m] and G_i is the initial shear modulus [MPa].

The larger the frequency of the signal, the more dampened the pile motion due to the soil effect (increase of the importance of imaginary part compared to the real part of the soil stiffness).

Holeyman (1984) supposes that the pile/soil system creates a plastic zone around the pile under large dynamic solicitations and this disturbed zone is located in the close vicinity of the pile shaft. So, the radiation is reduced and almost vanished when the plasticity rate increases. Holeyman takes this property into account by replacing the initial shear modulus of Equ. III- 18 by tangent shear modulus of the static stress-displacement relationship. Its evolution with η is given by:

$$G = G_i \cdot (1-\eta)^2$$ **Equ. III- 19**

- G is the local tangent shear modulus [Pa];
- G_i is the initial tangent shear modulus [Pa];
- η is the mobilization ratio [-].

The plastic slider

The plastic slider models the natural limitation of the soil resistance. This threshold is influenced by the loading rate and follows the well known non-linear velocity dependency as described in chapter 2.

$$\tau_{rheol} \le \tau_{ult,rheol} = \tau_{ult} \cdot \left(1 + J.v^{0,2}\right)$$ **Equ. III- 20**

The parameters J and N are set equal to those of the viscous term but they should be different (especially for the parameter J that determines a typically different behaviour).

2.2.2.3 The rheologic shaft soil reaction

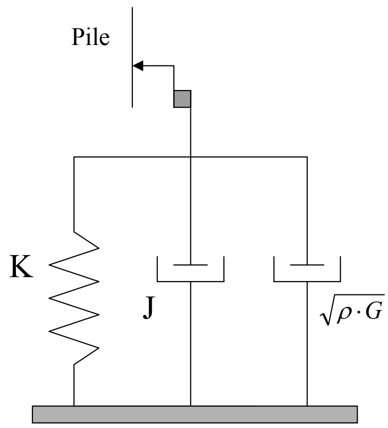

Figure III-4 : rheologic shaft model

The shaft friction model is summarized in Figure III-4. The static term is based on the hyperbolic law and the non linear stiffness k is related to the level of soil mobilization. It describes the low and large static strains. The first dashpot determines the viscous part of the soil reaction (relative to the loading rate effect). This dashpot is non-linear since the relationship is a power-law of velocity. The second dashpot represents the radiation damping. The dashpot is non linear since the shear modulus value decreases when the rate of mobilization increases. The slider is the rheologic ultimate resistance of the soil limiting the sum of all terms.

2.2.3 Base model

Similarly to the shaft modelling, the base model is composed of a static and a dynamic term which are described hereafter. The model is built to represent the soil response at low and large solicitations.

2.2.3.1 Small deformations under static and dynamic solicitations

As described in chapter 2 (section 4.2.1.), the base response is based for small strain Lysmer and Richart analogue (1966) that represents the response of an elastic half-space medium under harmonic solicitations applied on the centre of a circular and rigid footing resting on an elastic and homogeneous half-space (Figure III-5). The footing has a radius R, a mass m and the medium has an initial shear modulus G_i, a soil density ρ and a Poisson's ratio υ.

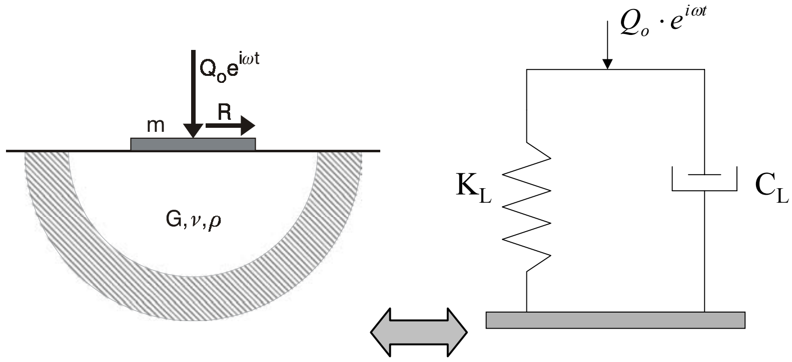

Figure III-5 : Lysmer analogue

The Lysmer analogue is composed of a spring for the static term of the reaction and a linear dashpot representing the energy losses by radiation in the soil beneath the pile base. This model can be applied to the pile base reaction by considering the footing radius as the pile base radius and the footing mass as the pile mass (without shaft effects). The stiffness and the dashpot factors are given by:

$$K_H = \frac{4G_i R}{(1-\upsilon)}$$ **Equ. II- 21**

$$C_H = \frac{3.4R\sqrt{G_i\rho}}{(1-\upsilon)}$$ **Equ. II- 22**

- K_H is the spring stiffness [N/m];
- C_H is the damping factor [Ns/m];

2.2.3.2 Large deformations under static and dynamic solicitations

Since the model based on the Lysmer analogue is only valid for homogeneous and elastic media. Holeyman (1984, 1985) modifies it to account for a heterogeneous half-space and a non-linear behaviour of the soil response. Figure III-6 represents an equivalent solid supposed to take account of these elements. The equivalent axisymetric solid rests below the footing and the model finally rests on a half-space medium governed by the analogue of Lysmer (K_H & C_H). The finite lateral extents are determined to have a correct response model under static and dynamic conditions (Holeyman, 1984). In this equivalent solid, only the vertical mode of deformation is considered and the cone mass density is equal to the soil medium. The vertical modulus of elasticity E_v is given by:

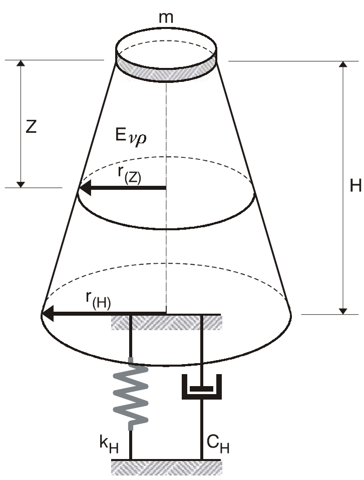

Figure III-6 : Concept of the equivalent solid (after Holeyman, 1988)

$$E_v = \frac{G_i}{0.85 \cdot (1-\upsilon)^2} = \frac{E_i}{1.7 \cdot (1-\upsilon)^2 \cdot (1+\upsilon)}$$ **Equ. III- 23**

- E_i is the initial modulus of elasticity [MPa];

This relationship is due to the respect of the equality between the impedances of the half-space medium and the equivalent solid section (Holeyman, 1984). The evolution of the cone radius r(z) is function of the depth z, the pile radius r_0 and the Poisson's ratio:

$$r(z) = r_0 + \frac{1-\upsilon}{\sqrt{0.85}} \cdot z$$ **Equ. III- 24**

This relationship is due to the combined action of the respect of impedances (dynamic condition) and the respect of elasticity condition (static condition) with the static settlement of the Lysmer analogue. The model has the advantage to be easily discretized in lumped parameter accounting for the local properties (non-homogeneity) of each layers (Figure III-7)

The cone is divided into n elements of same thickness and the stiffness used in the calculus correspond to those located in a mid position between two masses. An equivalent stiffness, similarly to Equ. III- 8 is used. Half an element mass is added to the pile last element and the last element before the half space has also a half mass. The base model does not accept tension stress; this is a direct consequence of the physical situation where the pile base acts in compression but not in tension. Consequently, the stress base response is set to 0 if the stress state beneath the pile base is in tension. The non-linear response of the soil, typical for large deformations, is integrated in the intermediate elements with the hyperbolic law (Kondner, 1963) adapted to the axial deformation and stresses.

This model is characterized by an elastic unloading phase (stiffness equal to the initial modulus) defining the hysteretic damping of the pile behaviour. This unloading path is defined as linear (with the same stiffness than the initial one, or modified similarly to the shaft model by using another stiffness ruled by a ratio E_i/E_2).

2.2.3.3 Viscous damping

A viscous effect is accounted for into the equivalent solid, function of the soil velocity and of the static soil reaction similarly to the shaft model.

$$\sigma_{rheol} = \sigma_{stat} \cdot \left(1 + Jv^N\right)$$ **Equ. III- 25**

Where J and N are the rheologic parameters of the base reaction.

The radiation damping

The radiation damping is accounted for by the geometry of the cone and the masses of the lumped elements. The behaviour at the base of the cone is assumed as low strain as sufficient in order to use the Lysmer analogue defined for an elastic behaviour.

The plastic slider

The plastic slider models the natural limitation of the soil resistance. This threshold is influenced by the loading rate and follows the well known non-linear velocity dependency as described in chapter 2.

$$\sigma_{rheol} \leq \sigma_{ult,rheol} = \sigma_{ult,stat} \cdot \left(1 + J.v^{0,2}\right) \quad \textbf{Equ. III- 26}$$

2.2.3.4 The rheologic base soil reaction

The model is summarised by Figure III-7.

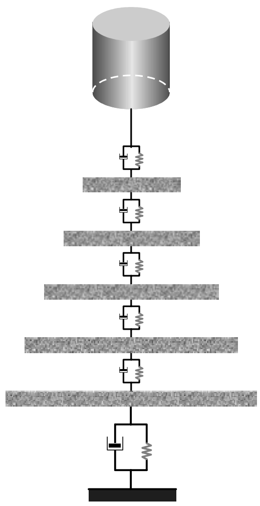

Figure III-7 : Rheologic base model

The soil response is given by an equivalent solid allowing heterogeneity and non-linearity lying on a half-space represented by a Lysmer analogue modelling the elastic response of the soil in the far field. The settlement of the base response is given by the settlement of the all cone and the settlement of the elastic half-space:

$$S_{\infty} = \Delta S + S_H \quad \textbf{Equ. III- 27}$$

- ΔS is the settlement of the cone;
- S_H is the settlement of the half-space medium.

The stress is given by the stress undergone by the first cone element. The inside model is composed of a spring of which the stiffness corresponds to the non-linear static soil response and is function of the mobilization ratio and the relative displacement between cone elements; the hysteretic damping is included. The damping represents the viscous and strain rate or velocity dependent term regarding to the relative motion between cone elements. The plastic slider accounts for the static ultimate soil resistance and the loading rate effects. The cone base reaction follows the Lysmer analogue.

2.2.4 Parameters management

The soil is described by layers for both shaft and base reactions. The number of layers is limited to 5 for both shaft and base resistances.

- Shaft resistance parameters: each layer is characterized by its depth z_i, the ultimate shear strength $\tau_{ult,i}$, the initial tangent shear strength G_i and the damping factor corresponding to both viscous and ultimate rheologic forms J_i. The unloading modulus G_2/G_1 is set for all layers.

- Base resistance parameters: each layer is characterized by the same set of parameters : z_i, $\sigma_{ult,i}$, E_i, J_i and a ratio E_2/E_1 for the unloading (for all the layers). The soil is also divided in layers even if the only parameters used are those of the layers intersected by the cone of soil. The coefficient of Poisson and the mass density are required for the cone set-up.

- Pile and model parameters: pile parameters required: geometry (radius, length, type of section, expanded base, …) and material description (elastic modulus, mass density,…) and model parameters required: the mathematical and processing assumptions impose a number of parameters as the number of pile elements, the description of the cone (number of elements, height), the duration of the studied signal or the time increment precision.

2.2.4.1 Set of parameters : Input and sorting

The values of the soil parameters are the main unknowns of the back analysis problem. They can be characterized by a level of uncertainty and a level of influence in the dynamic pile response evaluation. Each parameter has a proper weight determined by its influence on the pile model response. The first set of parameters is used to describe the pile/soil system and allows one to calculate a first response for a given solicitation. This first estimation of the parameters is based on different sources. The most common is to use the geotechnical information available on site. If some of them are missing, existing correlations with known parameters are possible.

The number of parameter to be optimised is too large and a rational approach has to be undertaken in order to reduce this number. One idea was to sort the parameters in categories based on the level of reliability of their values. The number of parameters is reduced and also the complexity of the process.

The parameters are classified by categories: pile geometric and mechanical data, geomechanical data, rheological data (load rate effects parameters), test data and modelling parameters.

The pile geometric data are known *a priori* for most piles to be tested. The level of certainty varies from high to medium if the pile is a prefabricated driven pile (every dimensions are known) or if the pile is a cast-in-place one with enlarged base. Some of the parameters could be optimised but in an independent process, using methods built for this purpose (like the integrity method,…). In general the pile geometric data in the back-analysis process are assessed as known parameters.

Laboratory tests, literature, direct analysis of the measured signals or personal experience can give a good knowledge *a priori* of the pile mechanical parameters. In function of the source, the reliability is more or less important. But since the methods can be compared, and the theory allowing the calculation of the different parameters well established, their first evaluation does not seem to be far from the real solution. These parameters are not integrated to the general back-analysis problem.

The geomechanical parameters defining the fundamental soil relationships are the main unknowns of the problem and also the main objective. Besides these parameters, the type of relationships chosen to model the pile/soil interaction is also one of the main assumptions. The whole back-analysis process, performed manually or automatically, is focused on these parameters. As explained before, laboratory tests or geo-technical *in situ* tests can give a first estimation but contrary to the pile properties, the soil characteristics are dependent of the stress history and the environment within they are evaluated. Laboratory tests, CPT tests or other resources cannot exactly reproduce the conditions in the soil after or during driving. This is a major reason why these parameters are highly uncertain and need a specific back-analysis in order to be evaluated in the field conditions[1].

The rheologic parameters (J and N) are linked to the loading rate effects. This behaviour is still poorly understood either for the specific value of J and N or for the behaviours they represent. Chapter 2 is focused on the research undertaken in this domain. Since these parameters (or preferably this behaviour) have a large influence on the dynamic load test results, the back analysis will try to estimate the best value for these parameters according to the assumptions of the chosen model.

The test data are function of the firm that performs the tests and the observation of the testing system before the dynamic loading test. Correlation with measurements made by transducers can confirm these values. They do not require an optimisation process.

The model parameters are connected to the numerical stability of the code, and the precision required for the results. They have to be chosen with discernment and do not have to be optimised.

Summary of the parameters

Figure III-8 presents a summary of the parameter classification and the importance to be accorded into the back-analysis process.

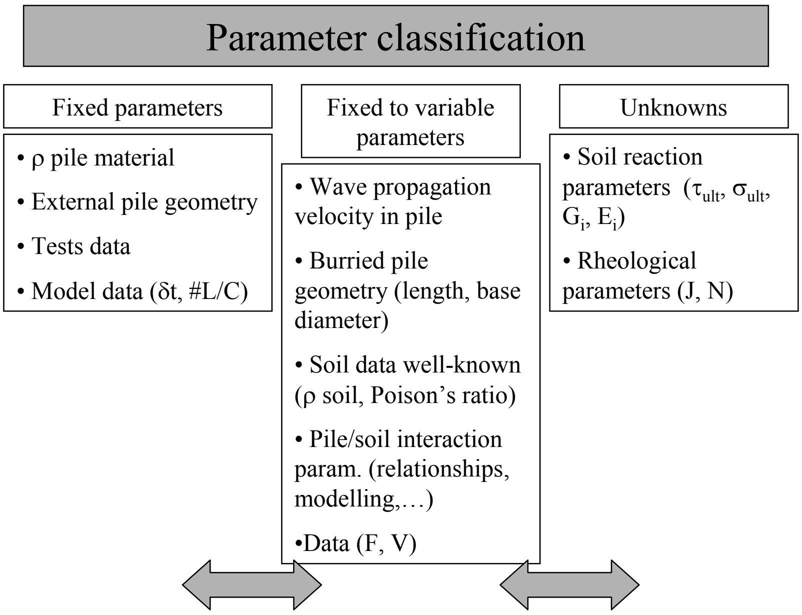

Figure III-8 : Classification of parameters according to their reliability

The arrows mean that the parameters located in the middle column can move from a position of variable parameter to fixed or unknown categories.

[1] Assumptions are made to equal the field conditions for static and dynamic cases (namely to compare the simulations of SLT with the real SLT). This can be partially correct for the installation influence but there remains a big uncertainty on the test consequences because of the loading rate effect on the soil state.

2.3. Algorithms – scheme of resolution – SLT simulation

2.3.1 The back-analysis process

The back-analysis process is fully described in chapter 5. It is based on the cross-matching of two signals (force and velocity measured at the pile head during the blow). These signals are compared to the corresponding model responses. An adjustment of the pile/soil parameters is performed in order to optimise the quality criterion. Once the matching fulfils the stop criterion, the soil's parameters are used to simulate the static load-settlement curve.

2.3.2 The static load-settlement curve simulation

The same pile/soil model is used to simulate the static load-settlement curve. The optimised set of parameters determined in the dynamic analysis is used to evaluate the bearing capacity of the pile under the constant settlement of the pile into the ground (from 10^{-2} to 10^{-5} m/s in order to have a simulation close to the real SLT). Consequently, the simulation is a constant rate of penetration test. The system solves the balances of forces at each node and at each time step for a monotonically increasing displacement. The soil reactions (shaft and base) are stored and the corresponding curves are plotted.

The modulus of elasticity of the pile used in the simulation is also different compared to the modulus used in the dynamic analysis. The empirical formulations of Mortelmans (1984) allowing to determine the dynamic and static elastic moduli from the concrete strength ($R'_{w,j}$) are used to evaluate the static modulus from the dynamic one introduced in the model for the dynamic analysis.

$$E_{stat} = 5200\sqrt{0.96R'_{w,j}}$$ **Equ. III- 28**

$$E_{dyn} = 5600\sqrt{0.96R'_{w,j}}$$ **Equ. III- 29**

$$E_{stat} = E_{dyn} \cdot \frac{5200}{5600} = 0.93 \cdot E_{dyn}$$ **Equ. III- 30**

2.4. Decomposition of the rheologic shaft friction stress into static and velocity dependent terms

2.4.1 Presentation

In order to illustrate the rheologic response of the pile/soil system and especially the order of magnitude of each term, a damped harmonic signal of velocity (frequency ω, damping ξ and initial velocity V_o) is imposed to the pile model similarly to a measured dynamic signal during a DLT test (Figure III-9). The pile is modelled with one rigid element and the soil is a sole layer characterised by:

- τ_{ult} = 0.2 MPa;
- υ = 0.35;

- G_i = 100 MPa;
- J = 1 s/m & N = 1;

The reference signal is given by:

$V(t)=V_o \cdot e^{(-\xi \omega t)} Sin(\omega t)$ → Velocity (Figure III-10) **Equ. III- 31**

$$U(t)=\int V(t)dt=\frac{V_o}{-\xi\omega}\cdot\omega\cdot e^{(-\xi\omega t)}\frac{\left(Sin(\omega t)-\frac{\omega}{-\xi\omega}Cos(\omega t)\right)}{1+\frac{\omega^2}{(-\xi\omega)^2}}$$ → Displacement (Figure III-10) **Equ. III- 32**

$$Acc(t)=\frac{\partial V(t)}{\partial t}=V_o\cdot\omega\cdot e^{(-\xi\omega t)}\left(-\xi\cdot Sin(\omega t)+Cos(\omega t)\right)$$ → Acceleration **Equ. III- 33**

- Vo = 1.45 m/s;
- $\xi = 0.233\ s^{-1}$;
- ω = 272 rad/s.

- V_{max} = 1.03 m/s
- u_{max} = 7.4 mm
- u_{min} = 5.05 mm
- a_{max} = 391 m/s²

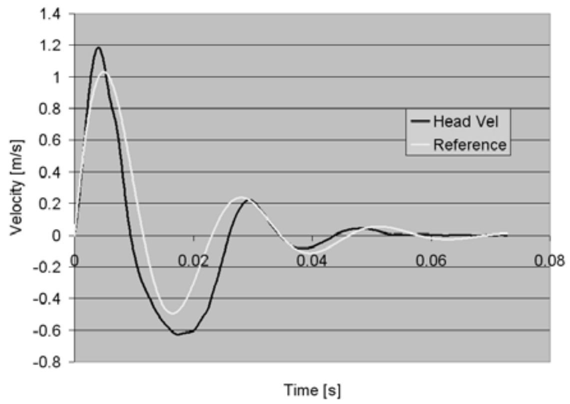

Figure III-9: Measured and reference velocities signals along the pile (blow B8-009 - Limelette)

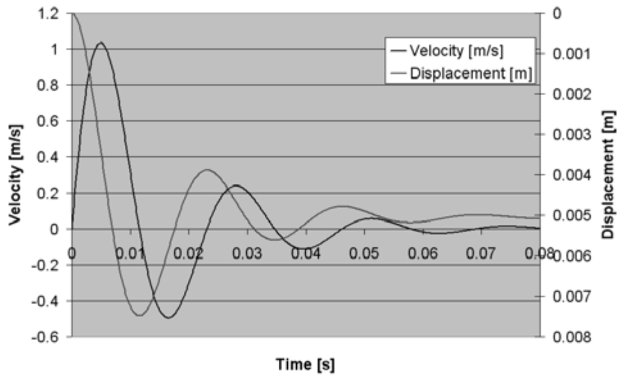

Figure III-10 : Plot of the reference velocity and displacement signals

The fundamental static stress-displacement relationship (Figure III-11) is hyperbolic and the rheologic soil resistance accounts for the static, the viscous and the radiation terms, all of them being limited by the velocity dependent rheologic ultimate stress. The tangent stiffness degrades with the soil mobilization towards the stress asymptotic value = 0.2 MPa and the unloading path is linear until the stress becomes negative. Afterwards, the hyperbolic progression starts again in the opposite stress sign.

Figure III-12 shows the terms of the rheologic stress already presented in the model: the static, the viscous and the radiation one (noted T_{stat}, T_{visq} & T_{rad} for τ_{stat}, τ_{visq} & τ_{rad}). The progression of the radiation stress is very fast and very stiff due to the high value of the radiation damping factor $\sqrt{\rho G}$ in the first part of the mobilization (when G is not degraded yet). After, with the progress of the static mobilization, the radiation damping decreases even before the velocity has reached its peak and the relative influence of the radiation damping decreases.

The viscous effect is relatively low, directly connected to the velocity and proportionally to the static soil reaction. The sum of all terms is also plotted and is mainly led by the radiation damping at the very beginning with a strong influence on the initial stiffness. This is also observable on the pile load testing dynamic curves. The soil material is characterized by an intrinsic resistance ($T_{rheol,ult}$), also velocity dependent to account for the load rate effect. This limit can never be exceeded by the sum of three terms. If the case happens, the value taken into account in place of the sum is the theoretical threshold. Figure III-13 represents the plots of the theoretical formulation of this limit and the sum of three terms.

The model uses the minimum value of those both terms (the yellow trace) also called the ultimate soil reaction. The rheologic term equals the static one when the velocity vanishes and there are angular points in the radiation trace when the static curve changes its behaviour from loading to unloading because of the change from hyperbolic loading to a linear unloading.

2.4.2 Observations

The break point in the progress of the rheologic soil reaction (green circle on Figure III-13) highlights the evolution of the soil mobilization from a continuum state (description of the intrinsic stress-displacement and velocity relationships) to a failure mode (slippage of the pile into the soil→ slider). Moreover, the failure occurs for very low static mobilization.

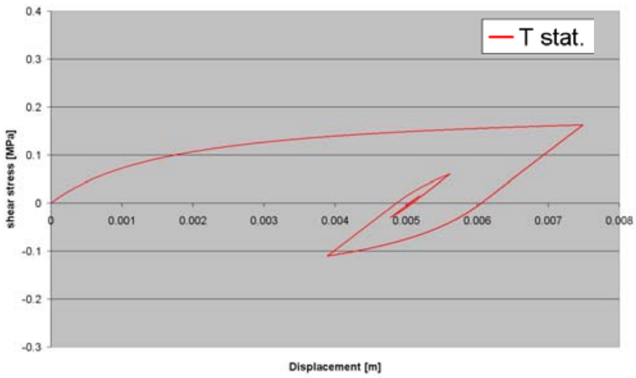

Figure III-11 : Static shear stress-displacement curve

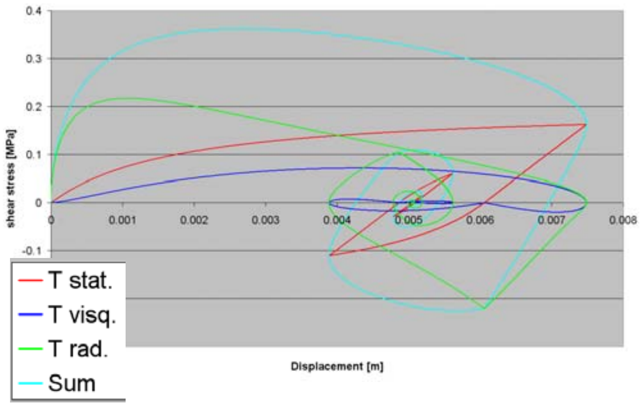

Figure III-12 : Static, viscous and radiation shear stress-displacement curves + sum of the three terms

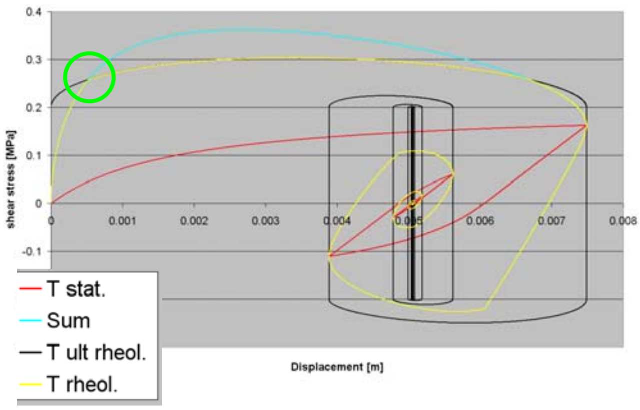

Figure III-13 : Static shear stress-displacement curve + sum of the three terms (static + viscous + radiation) + ultimate rheologic soil resistance + used rheologic stress-displacement curve

Figure III-13 expresses that the radiation has a strong and quick influence on the failure and the time needed to reach failure. The rheologic soil reaction appears to be almost linearly velocity dependent during the first part of the loading directly followed by a non–linear power relationship of velocity expressed by the formulation of the ultimate rheologic resistance when the limit of resistance is exceeded. Since this breakpoint and the relative dependency of different terms is conditioned by the loading rate and the mobilization rate, it could be interesting to investigate the influence of different loading rates on the rheologic stiffness from the start of mobilization until failure. This break in the continuity of the rheologic soil reaction could also be interpreted as a quake (without knowledge of the radiation damping). However, the quake is linked to the static and intrinsic behaviours of the soil, whereas this event is rather related to the velocity and the level of static mobilization. Both behaviours are linked to the passage from soil mobilization state to failure mode but the former is connected to the displacement field (the quake), and the 2nd to the velocity field.

The influence of the velocity dependent terms is significant for the measured applied load and the deduced soil reaction but both terms (viscous and radiation terms) influence also the initial stiffness of the stress-displacement curve that can be easily compared to a load-settlement curve without taking the inertial effects into account.

2.4.3 Influence of a variation of the velocity and frequency of the loading signal

Since the loading description has a strong influence on the form of the load-settlement curve (especially at the very beginning), it is proposed to investigate the effects on the initial stiffness of a variation of velocity amplitude V_0 and frequency ω that modify both loading duration and magnitude. The velocity signal described in section 2.4.1. (Equ. III- 32 to Equ. III- 33) is imposed to the pile in contact with one soil layer. Obviously, both of them influence the time needed to generate a given displacement, the higher or the longer the maximum velocity, the longer the displacement mobilized.

2.4.3.1 Variation of magnitude

The velocity synthetic signal is limited to the first half phase (Figure III-14). The velocity starts from zero, increases until its maximum and decreases to zero. The signal evolves by modifying V_0 from 0.2 to 2 m/s. The plots of displacement & velocity vs. time, velocity vs. displacement and soil reaction vs. displacement are displayed on Figure III-14 to Figure III-17. The displacement curve is a damped cosinus characterised by the same parameters (ω, ξ and V_o).

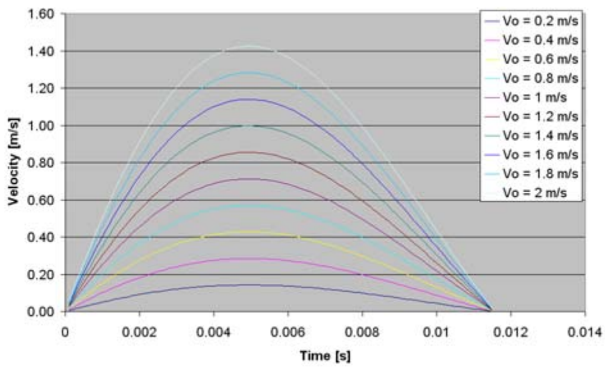

Figure III-14 : Variation of Vo: Velocity vs. time

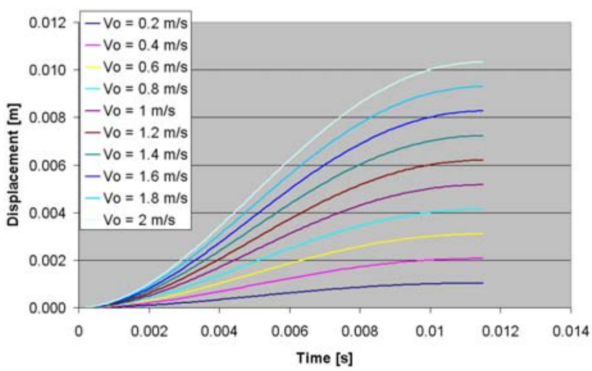

Figure III-15 : Variation of Vo: Displacement vs. time

The rheologic stresses (Figure III-17) are evaluated by the superposition of the static, the viscous and the radiation terms limited by the velocity dependent ultimate rheologic resistance and the radiation term is function of the mobilization ratio.

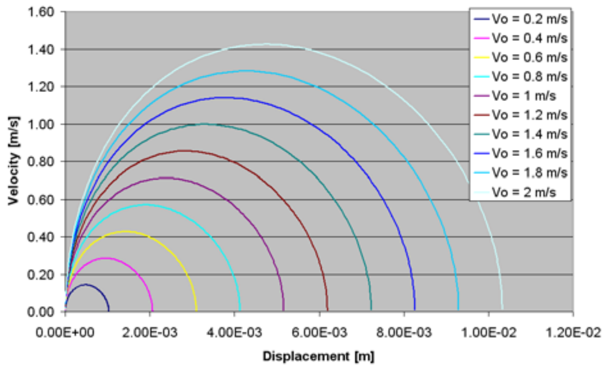

Figure III-16: Variation of Vo: Velocity vs. displ.

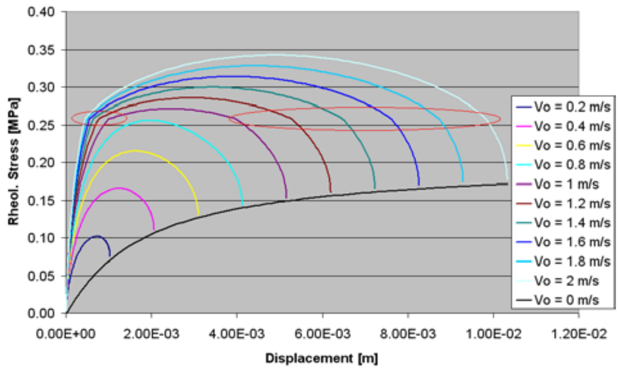

Figure III-17 : Variation of Vo: Stress vs. displ.

The red ellipses on Figure III-17 surround the break points defining the passage from the description of the continuous media to the failure mode (and the slippage conditions). This failure zone is conditioned by Equ. III- 34 also illustrated in the velocity-stress plot (Figure III-18). This last figure highlight the fact that there is a limiting value v_{lim} of the velocity corresponding to the failure or the beginning of the slippage.

$$\tau_{stat,ult}\frac{s}{s+\dfrac{\tau_{stat,ult}}{G_i}}\left(1+J\cdot v_{\lim}\right)+\left(1-\frac{\tau_{stat}}{\tau_{stat,ult}}\right)\sqrt{G_i\cdot\rho}\cdot v_{\lim}=\tau_{stat,ult}\cdot\left(1+J\cdot v_{\lim}\right)$$ **Equ. III- 34**

- s is the displacement [m];
- G_i is the initial tangent shear modulus [MPa];
- τ_{stat} is the static stress [MPa].
- ρ is the mass density [kg/m³];
- J is the damping factor [s/m].

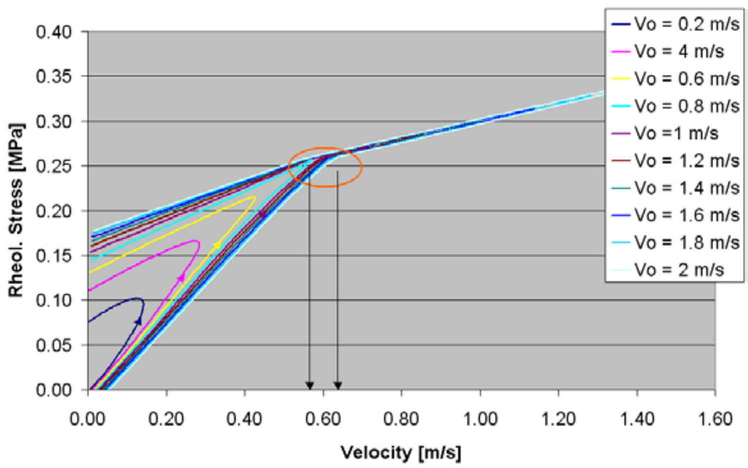

Figure III-18: Variation of Vo: Stress vs. velocity

This range of velocity concerned by the failure passage is very narrow and can be thought as characteristic of the chosen pile/soil model. The difference of behaviour characterizing the state before and during the failure is also well pronounced with the evolution of the curve slopes. The failure zone appears to be linear due to choice of N=1 in the imposed pile/soil model. The influence on the resulting initial stiffness of the stress-displacement curve is pronounced even for low velocities (compared to the equivalent static curve).

2.4.3.2 Variation of frequency

After the analysis of a variation of velocity magnitude V_0, next observation concerns the frequency ω in order to lengthen the duration of the load application (ω varies from 25 to 300 rad/s). The velocity magnitude is kept constant. The velocity and displacement vs time and stress-displacement relationship figures are given in Figure III-19 to Figure III-21. The generated displacements are displayed in Figure III-20 with a longer duration and a larger reached displacement for simulations performed with a smaller frequency.

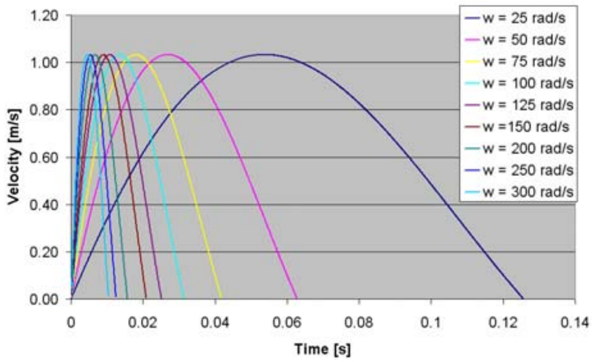

Figure III-19 : Variation of the frequency of the synthetic velocity signal

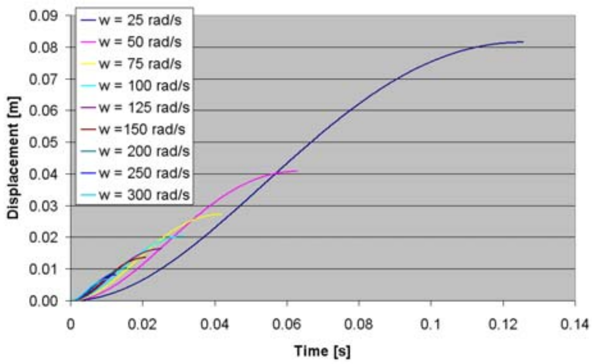

Figure III-20 : Variation of the frequency of the velocity : influence on the generated displacement

Since the maximum velocity is kept constant, the lengthening of the loading means an increase of energy transmitted to the pile and consequently a larger displacement and soil mobilization.

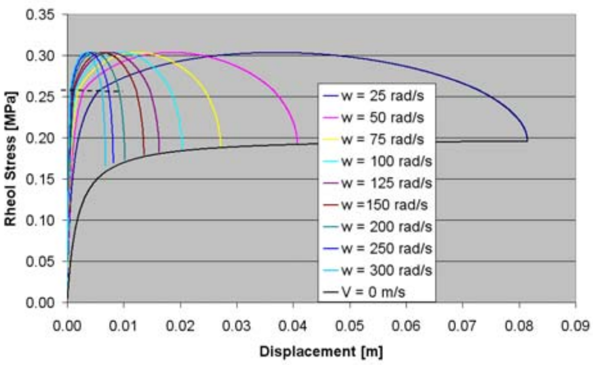

Figure III-21: Variation of the frequency of the velocity : influence on the mobilized rheologic stress

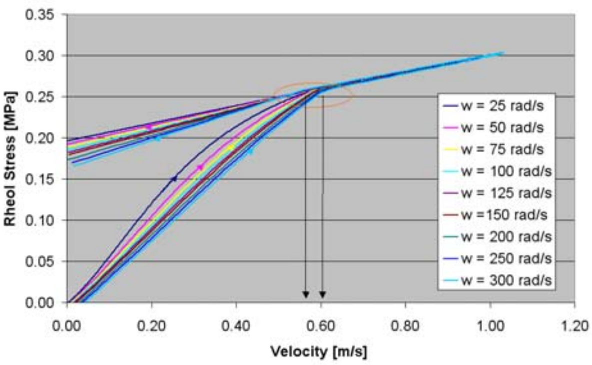

Figure III-22: Variation of the frequency of the velocity: velocity vs. rheologic stress

Equally to the previous case, Figure III-21 and Figure III-22 highlight the variation of initial stiffness, the narrow range of velocity for which the soil slippage condition kicks in (about 0.6 m/s).

3. Dynamic load test measurement: project description and signal analysis

After the description of the pile/soil model including the fundamental relationships, the parameters classification and the particular attention put on the rheologic stress and its developments, the focus is set on the real measurements performed on field. These data are here described. First, the projects from where the measurements were extracted are shortly described with a special attention to the geotechnical data usable in this research. After, a strict analysis of the maximum quantities measured is proposed with relationships existing between measured force, velocity, energy and settlements. Finally the quality of the signal is introduced in order to appreciate the sensitivity of the result only based on the quality of the measurement.

3.1. The Screw Pile projects

3.1.1 Genesis of the project

Within the framework of the setting-up of the Eurocode 7 relating to the Geotechnical Design, the Belgian Building Research Institute (BBRI) has organised in 1998 an ambitious research program with the financial support of the federal Ministry of Economic Affairs aiming to involve all Belgian piling companies installing cast in situ soil displacement screw piles plus representatives of organisations concerned by foundation design. The main topics of this program were to execute an experimental test campaign with cast-in-place screwed piles able to lead a proposal of semi-empirical design methods using installation coefficients. This program is organised equally in two representative types of soil encountered in Belgium: the tertiary overconsolidated Boom clay and a sandy bearing stratum (Bruxellian sand) underlying soft sedimentary layers.

3.1.2 Sint-Katelijne-Waver program

In the Boom clay site at Sint-Kathelijne-Waver (Belgium), 5 existing screw piles systems plus precast driven piles[2] without base enlargement were installed with the purpose to be tested dynamically and statically and by the statnamic method (intermediate loading rate or kinetic loading – Middendorp (1992)). Before the pile installation, an extensive geotechnical survey has been carried out on the site with most of the tools used by laboratories and contractors and required for design: Cone Penetration Tests (CPT) (including different types of cone and process), Standard Penetration Tests (SPT), Pressuremeters Tests (PMT), Dilatometers Tests (DLT), geophysical tests (SASW, seismic cone, seismic refraction) and a boring with undisturbed samples allowing for laboratory tests. Integrity testing of the piles was also carried out. Due to the Belgian practice, the CPT tests represented the largest part of the available information. A huge amount of analysis and most of the results have been compiled in the proceedings of the symposium organised in Belgium in 2001 (Holeyman, 2001).

Schittekat (2001) describes in detail the Boom clay under several aspects (geology, stratigraphy, geomechanic and geotechnical characterization). The Rupelian clay, or Boom clay is a marine deposit

[2] The precast pile is considered as the reference for Belgian design methods

of Middle Oligocene age (35 m.y.). The total thickness of the original clay formation could have been well above 100. Later erosion has removed part of the clay to leave typical thickness of 70 m in Antwerp. The removed overburden in the Antwerp area is estimated to be 90m. Consequently, the Boom clay may be considered as an overconsolidated clay.

Geological observations show the existence of fissures, diapir structures and septaria all related to the stress relief. These features might be at the origin of the scatter of the results of the *in situ* tests. It is admitted that cone resistance values of a CPT should steadily increase with depth in stiff fissured clays and remains in the range of 2.8 MPa to 4.4 MPa.

The testing site is 50x25 m² and was completely covered by all the investigation tests performed. The site layout is described in Figure III-23.

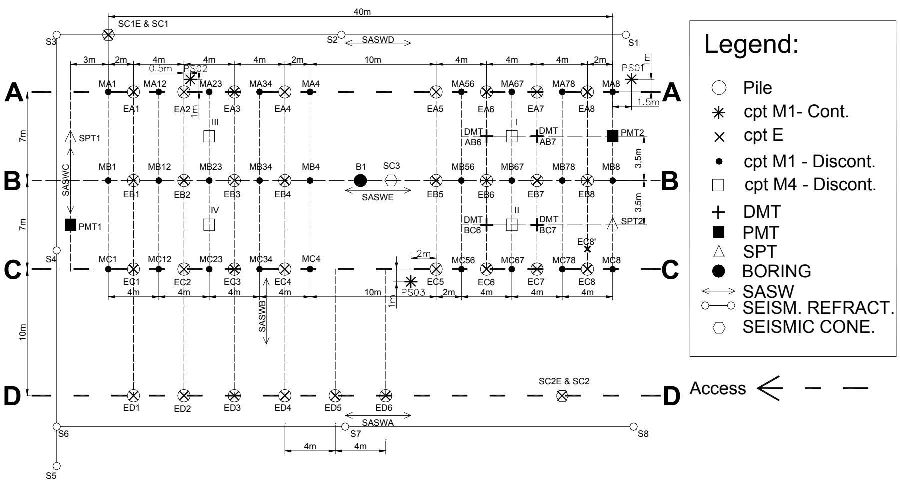

Figure III-23 : Sint-Katelijne-Waver : testing area layout (after Mengé, 2001)

3.1.3 Limelette program

In the second phase of the BBRI research program, a similar test campaign was organized in Limelette (Belgium) where the subsoil consists of 8 m of quaternary silty layers (loam) and tertiary Ledian-Bruxellian sand. The groundwater can not be found in the shallow layer layers investigated. A similar testing program than for the clayey site was followed: 30 pile load tests composed of 12 static load tests, 12 dynamic load tests and 6 statnamic tests. Besides this load testing program, an extensive soil investigation campaign was still organized with CPT, SPT, PMT, DLT, geophysical tests and a boring with undisturbed samples (lab tests) during different phases of the project. Similarly to Sint-Katelijne-Waver, a symposium was organised in 2003 in Brussels (Huybrechts and Maertens, 2003) wherein all the information and the analysis about the pile loading and the geotechnical campaigns are abundantly described.

Between the Asse Clay and the Ypresien clay layers, the layer of Brusselian sand (a serie of Lutetian sand) outcrops in the area of Brussels (Belgium). This sand results from a deposit during the Eocene age in a coastal area of probably a tropical sea. The layer is about 50 meters thick and presents a large panel of different sands with different grain size distribution, grain shape and carbonate content. The layer is more or less horizontal with a gently slope towards the North. These sediments are covered by quaternary silts formations with a thickness up to 6 m. The Brusselian sand is characterized by numerous facies changes not only at a regional scale but also at a local scale.

The test layout is organised similarly to the Sint-Katelijne-Waver site in order to reduce the risk of variability of soil properties due to distance. The site is divided in two parts: a static test field where the static load tests were performed and a dynamic test field designated for the dynamic load and statnamic tests.

3.1.4 Sites Characterization

3.1.4.1 Sint-Katelijne-Waver

The tests results presented herein are those used in the present research: CPT results - geophysical conclusions (wave propagation velocity V_s and shear modulus G_o) - physical characteristics of the soil.

CPT results

The CPT results presented on Figure III-24 and Figure III-25 show typical CPT profiles from both sites. The traces represent the envelopes of 30 and 18 tests, respectively. The scatter is more pronounced for the silty site than for the clayey one. Both q_c and f_s results (cone resistance and local shaft friction) will use as input set of data for the pile/soil interaction back analysis procedure (see chapter 5). R_f is the ratio of f_s on q_c.

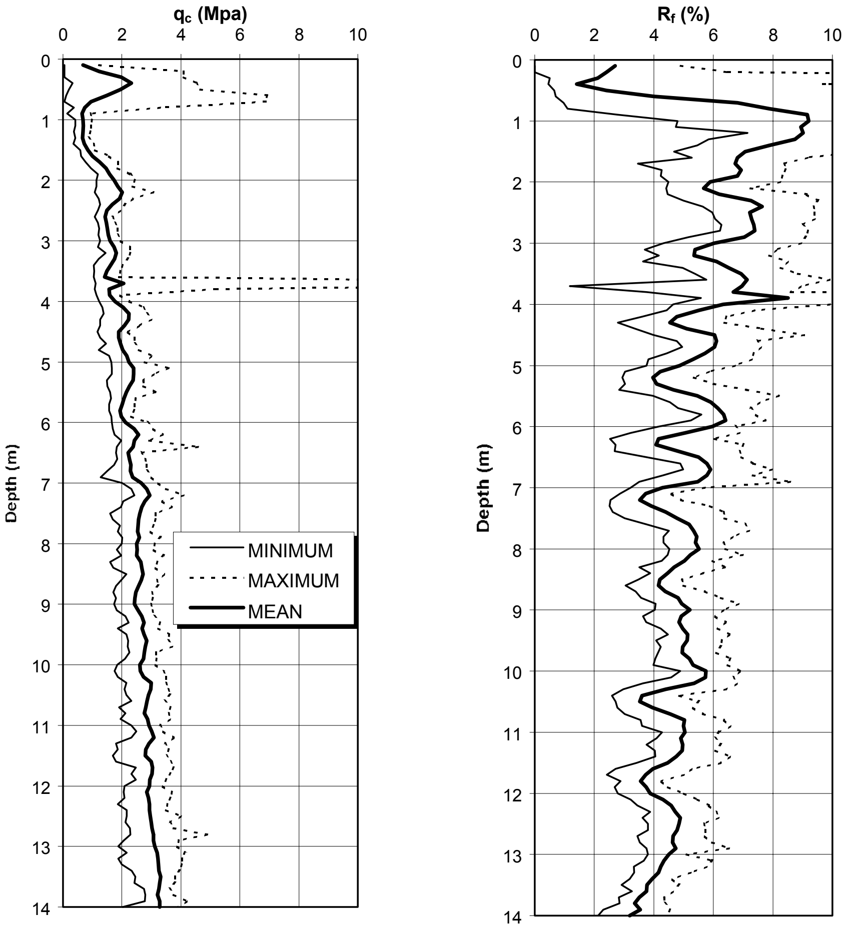

Figure III-24 : Mean, min and max q_c and R_f values from Sint-Katelijne-Waver (after Mengé, 2001)

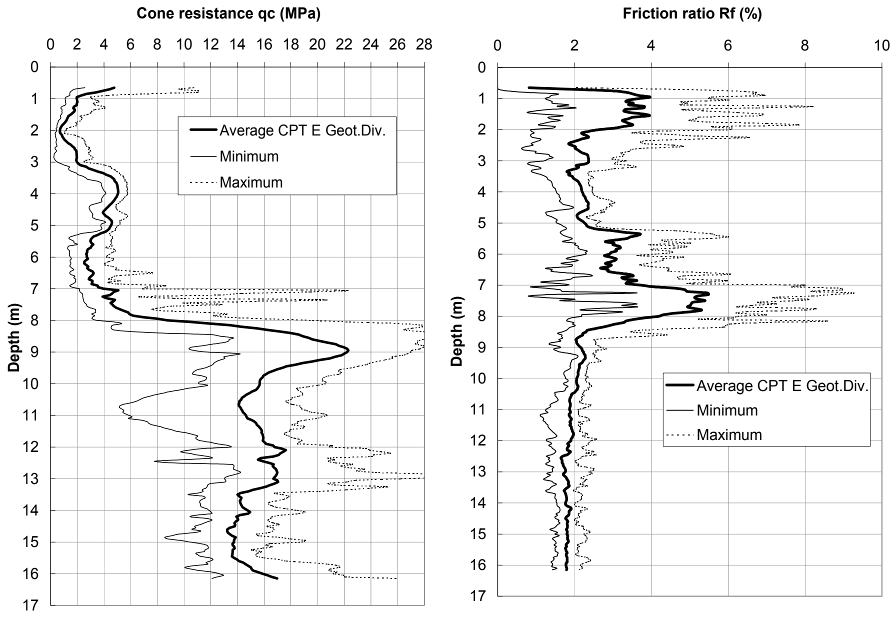

Figure III-25 : Mean, min and max q_c and R_f values from the dynamic test field of Limelette (after Van Alboom & Whenham, 2003)

Geophysical investigation

The values of G_o presented in Figure III-26 and Figure III-27 summarize the results of 3 geophysical *in situ* tests and 1 lab test:

- The seismic cone penetration test;
- The seismic refraction tests;
- The SASW test (Surface Analysis of Surface Waves).
- Laboratory tests, namely triaxial tests (Bender elements).

When studying Figure III-26 and Figure III-27, a large scatter of G_o values is found for both sites. It is known that V_s and consequently G_o are influenced by several factors: the main direction of the particle movement or the anisotropy of the studied soil, the stress level, the soil density and the soil structure.

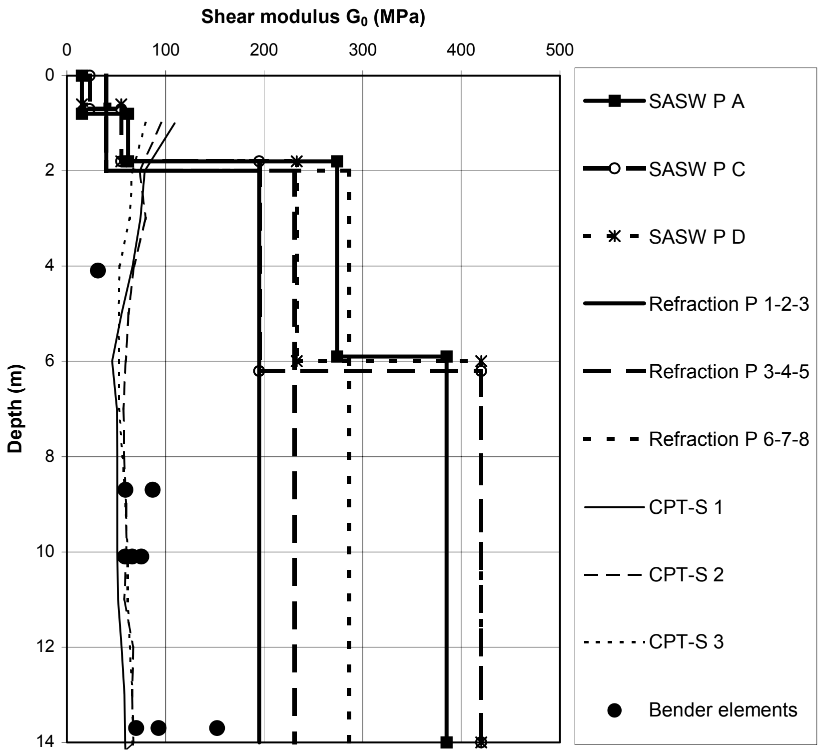

Figure III-26 : Shear modulus G_0 derived from in situ and laboratory seismic tests (Sint-Katelijne-Waver) (after Mengé, 2001)

The particular over-consolidated state of the Boom clay could be involved in the scattering shown in Figure III-26.

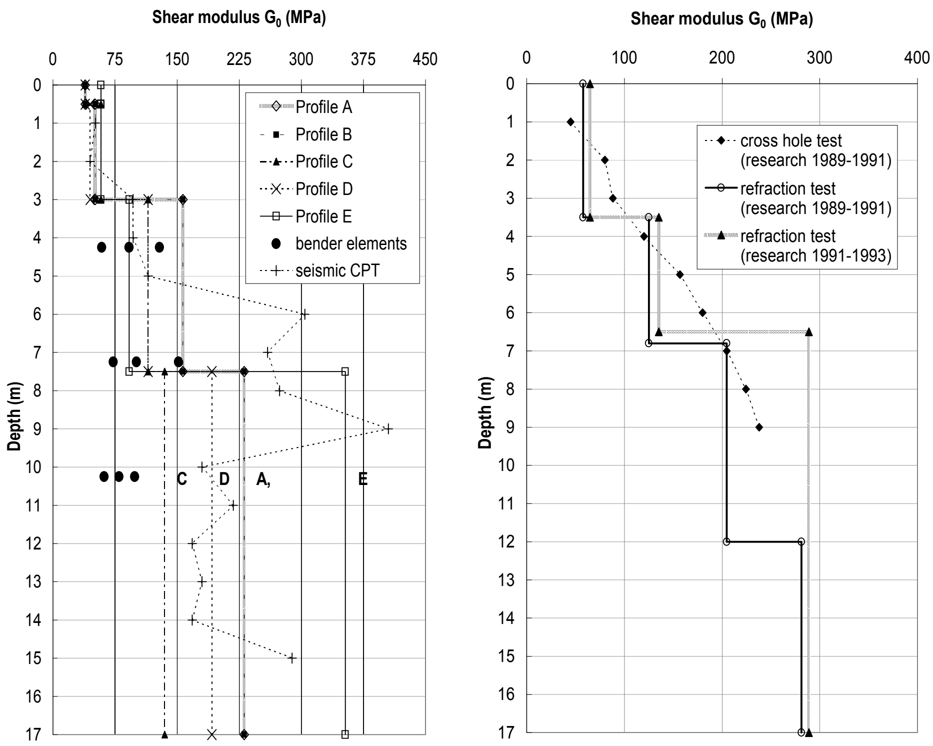

<u>Figure III-27</u> : Shear modulus G_0 derived from in situ and laboratory seismic tests (Limelette) (after Van Alboom & Whenham, 2003)

In Limelette, seismic refraction tests were performed in 1989-1991 and 1991-1993 at a distance about 50m to 150m from the test site. Also a cross hole test was conducted during the research project of 1989-1991. The concordance between both methods is very good and remains also in accordance with SASW results of the 2002 research (<u>Figure III-27</u>).

The G_o profile is extremely uselful for the interpretation of dynamic load test in the description of the fundamental soil relationships.

Boring and laboratory tests

<u>Table III-1</u> provides the results obtained for the UU and CU-triaxial tests of Sint-Katelijne-Waver. The watertable at the test site is found at 0.5 m to 1.0 m below ground level.

Characteristic	Sample depth 4.50 m – 4.90 m	8.50 m – 8.90 m	10.50 m – 10.90 m	13.50 m – 13.90 m
γ_d (kN/m³)	15.7	15.3	15.5	15.4
γ_n (kN/m³)	19.7	19.3	19.5	19.4
w (%)	25.3	26.0	25.8	26.1
Sr (%)	(101.8)	99.2	(100.9)	(101.0)
w_L (%)*	72.2	65.1	75.9	71.8
w_P (%)*	25.4	25.3	26.2	26.0
I_P (%)*	46.8	39.9	49.7	45.8
φ' (°)	26	28	26	27
c' (kPa)	20	30	40	15
c_u (kPa)	88	129	158	188

<u>Table III-1</u> : Physical characteristics and results of triaxial tests of the Boom Clay at Sint-Katelijne-Waver (after Mengé, 2001)

(*) These tests were performed on samples recovered 0.50 m higher.

Table III-2 provides the main results of the physical tests and the results obtained for the CU and CD triaxial tests of the Limelette site. The watertable at the test site is not found.

Characteristic	Sample depth 4.00 m – 4.50 m	7.00 m – 750 m	10.00 m – 10.50 m
γ_d (kN/m³)	16.4	18.4	13.8
γ_n (kN/m³)	18.8	20.8	15.0
w (%)	14.8	12.9	9.0
Sr (%)	67.6	82.3	27.0
w_L (%)*	27.6	30.2	23.4
w_P (%)*	18.7	15.0	20.7
I_P (%)*	8.9	15.2	2.7
φ' (°) CU	34	34	34
φ' (°) CD	35	-	35

Table III-2 : Physical characteristics and results of triaxial tests of the Bruxellian sand at Limelette (after Van Alboom & Whenham, 2003)

3.1.5 Pile Loading Tests

Within the present research, the pile load tests data used from dynamic and static tests only concern the prefabricated pile type considered as reference in the BBRI projects. The reasons of this choice was the wish to limit the size of the treatments to be processed, the need of a certain homogeneity in the data and results and to limit the uncertainty linked to the cast-in-place piles. Moreover, the knowledge of the exact geometry and the mechanical properties of the prefabricated piles is a great help for the interpretation. The following information is required to use, describe and model the pile:

- A geometric and a mechanical description of the installed piles;
- A presentation of the static load results.

The geometric and mechanical description of the concerned piles is available in chapter 4. The 3 static tests involved in this research (comparison with the simulations issued from the dynamic analysis) are displayed in Figure III-28 to Figure III-30.

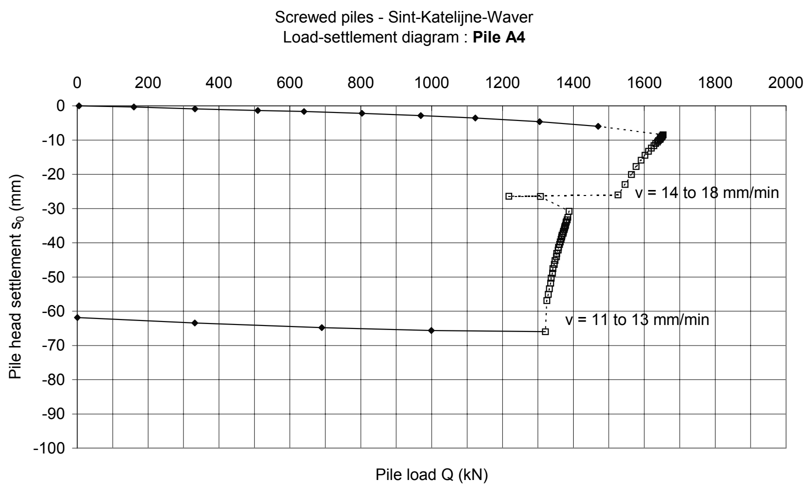

Figure III-28 : Load-settlement plot - Driven prefab pile A4 (SKW) (after Maertens & Huybrechts, 2002)

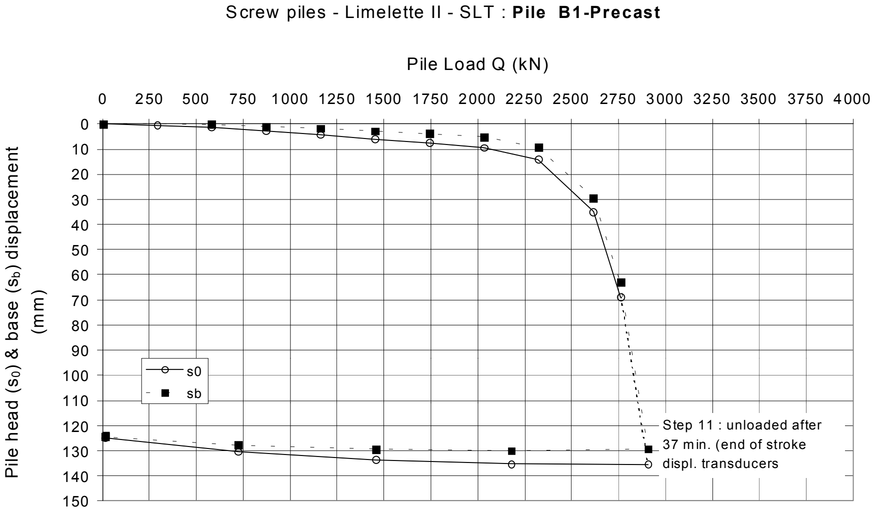

<u>Figure III-29</u> : Load-settlement plot - Driven prefab pile B1 (Lim.) (after Maertens & Huybrechts, 2003)

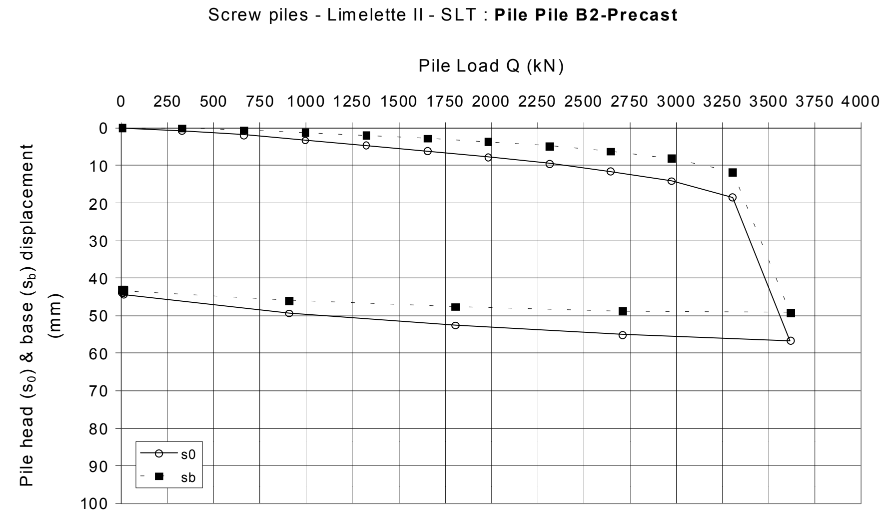

<u>Figure III-30</u> : Load-settlement plot - Driven prefab pile B2 (Lim.) (after Maertens & Huybrechts, 2003)

◆ = pile head settlement at the end of a constant loading, unloading or reloading step;

❍= pile head settlement during failure of the pile under a constant pile head penetration rate;

□= pile head settlement during failure of the pile under a non-constant pile head penetration rate.

A dashed type of line has been used to connect the last completed (after 60 minutes) load step (indicated with the symbol ◆) with the next non completed load step during which failure occurs (indicated with symbols ❍ or □), as well as for the connections between the points illustrating the failure of the pile.

3.2. Pile presentation

This section is focused on the study of data directly measured on field during dynamic loading tests (DLT). This presentation summarizes the main characteristics of these signals. So as to be precise in this description, it concerns only one kind of pile: the long prefabricated concrete pile driven into the soil a few month before testing. The advantages to only present the results of this pile are numerous:

- The pile geometry is known and equal for all piles: length, diameter all along the pile;
- Except for a failure during driving, the mechanical quality of the pile is assessed over the all length (no weak zone in the concrete strength profile);
- The concrete in all piles of a same site has similar properties and the same age;
- The pile driving provides dynamic data to be compared with the specific testing;

Consequently, the study of these piles reduces the number of potential unknowns and allows a fine comparison between piles which is more difficult with cast-in-place screwed piles.

The same model of pile has been driven in Sint-Katelijne-Waver (called “SKW”) and Limelette (called “Lim”). No pile head has been installed on pile during driving and for dynamic pile testing. The piles are 13 m (SKW) and 11 m (Lim) long, with a square section of 35x35 cm² .

The length dimensions are summarized in Table III-3:

	Static Load Test		Dynamic Load Test		Statnamic Load Test	
	SKW	Limelette	SKW	Limelette	SKW	Limelette
Buried length [m]		Variable-D	Variable-D 10.88	Variable-D 8.7 – 8.71	Variable-D 10.8	Variable-D 8.73
Distance transducer -base		9.8	12.2	9.8 – 9.8	12.2	9.8
Radius [m] shaft-base		0.446 0.395	0.446 0.395	0.446 0.395	0.446 0.395	0.446 0.395

Table III-3 : Summary of the dimensions of the prefabricated piles

- The buried length corresponds to the depth of base minus the excavation depth;
- “Variable-D” corresponds to the variable buried depth reached during driving.

There are two long piles tested dynamically in Limelette and one in Sint-Katelijne-Waver.

The dynamic data available for the study are for Sint-Katelijne-Waver:

- 7 drops in 1999 and 13 one year later.

And for Limelette:

- 16 drops for the pile B8 and 20 for the pile B9.

3.3. Relationships between maximum quantities

3.3.1 Heights of drop and dynamic settlements

The dynamic loading tests can be summarized by the schedule of drop heights. This height is related to the transmitted energy, the maximum velocity and also the settlements observed during the tests. The heights of drop during a testing procedure are generally increasing with an alternating succession of smaller drop heights. Table III-4 summarizes the dropping schedule for both sites and concerned piles.

	A7 – SKW (99)	**A7 – SKW (00)**	**B8 - Limelette**	**B9 - Limelette**
Blow No	**Drop Height [m]**	**Drop Ht. [m]**	**Drop Ht. [m]**	**Drop Ht. [m]**
1	0.4	0.2	0.4	0.4
2	0.8	0.4	0.6	0.6
3	1.2	0.6	0.8	0.6
4	0.8	0.6	0.8	0.8
5	1.2	0.6	1.0	1.0
6	1.6	0.8	0.6	0.6
7	0.8	1	1.2	1.2
8		0.7	0.8	1.2
9		1.2	1.4	1.2
10		0.7	0.6	0.8
11		1.3	1.6	1.4
12		0.6	1.0	0.6
13		1.4	1.8	1.6
14			1.8	1.0
15			2.0	1.8
16			2.0	1.8
17				2.0
18				2.2
19				2.6
20				2.6
Min	***0.4***	***0.2***	***0.4***	***0.4***
Max	***1.6***	***1.4***	***2.0***	***2.6***

Table III-4 : Summary of the drop heights (dynamic loading test results)

The height ranges are 1.4 m wide in clay up to 2.2 m in sand. This is due to the estimated bearing capacity and the concrete strength not to be exceeded in order to keep safe the pile integrity.

This section proposes a short analysis of the maximum and permanent displacements generated by the blows on the piles. Table III-5 and Table III-6 give the settlements evaluated from the signals, Figure III-31 and Figure III-33 illustrate the curves giving these values and Figure III-32, Figure III-34 and Figure III-35 summarize the results as pile displacements versus drop heights.

Beforehand, it is important to explain that the settlements occurring during the dynamic loading test are not measured but evaluated from the measured acceleration signals. Consequently, a correction is sometimes (often) performed in order to correct for the hypothetic errors of derivation due to the integration constants. It appears that the maximum displacement “measured” does not vary with these corrections, contrarily to the permanent displacement. This is due to the double integration process and the fact that the final settlement is evaluated at the end of the recorded signal (~ 0.2 s) more influenced by the corrections made. A fair confidence is given to the maximum settlement listed, and a slight variation is possible around the permanent settlement. However the trends remain valid.

Blow No	**A7 – SKW (I) Max Setl. [m]**	**A7 – SKW (I) Perm Setl. [m]**	**A7 – SKW (II) Max Setl. [m]**	**A7 – SKW (II) Perm Setl. [m]**
1	3.6	0.3	2.1	0.1
2	6.2	1.2	3.9	0.2
3	8.6	2.7	5.2	0.3
4	6.6	1.2	5.2	0
5	9	3.1	5.3	0.6
6	10.9	3.9	6.7	1.2
7	6.8	1	7.9	1.6
8			6.5	1
9			9.6	3.2
10			6.5	1.2
11			10.5	3.6
12			5.8	0.2
13			10.9	3.5
Min	***3.6***	***0.3***	***2.1***	***0***
Max	***10.9***	***3.9***	***10.9***	***3.6***

Table III-5 : Maximum and permanent settlements during DLT for SKW site

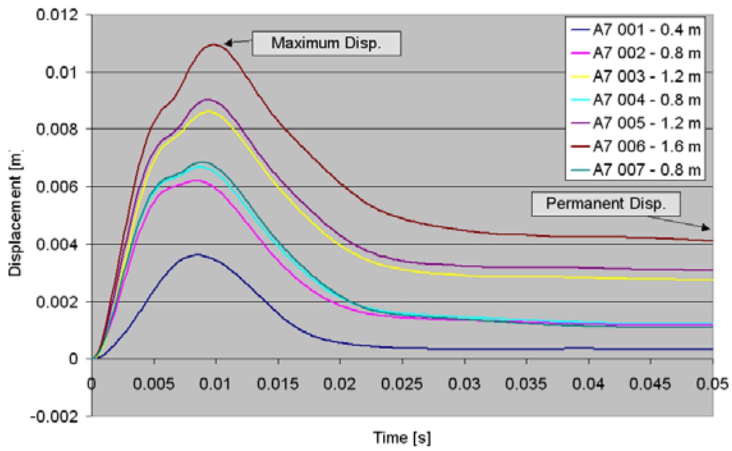

Figure III-31 : Plot of the displacement curves for A7 (99) of SKW

The curves of Figure III-31 present the displacements of the 1st set of tests performed in 1999. The influence of the drop height is evident, for both amplitudes and curve shapes. Moreover, the curves corresponding to similar drop heights provide similar responses. The curves are quickly dampened, with no subsequent oscillations after the first loading and unloading. This is due to the clay damping behaviour.

Figure III-32 represents the evolution of the maximum and permanent settlements (Table III-5) vs. drop height (Table III-4). This kind of figure is useful in the driving analysis. It allows the evaluation of the rebound of the pile (difference between permanent and maximal settlements) and the height required to obtain a given pile settlement.

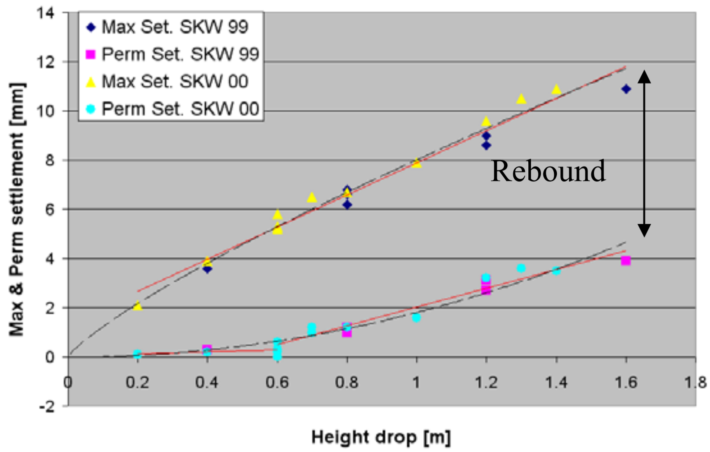

Figure III-32 : Heights of drop vs. maximum & permanent settlements (pile A7 - SKW)

The maximum settlement curves are characterized by a downward slope from the origin up to a given drop height and a constant slope for any superior drop heights. The permanent settlement curves are characterized by a null slope from the origin followed by an upward slope until both curves (max and perm settlement curves) becomes almost parallel (dashed lines on Figure III-32). This point, from where the maximum and permanent settlement curves evolve in parallel, is called the critical height h_c (Holeyman, 1984). Consequently, all tests carried out with a height drop inferior to approximately 0.6 m have no chance to generate permanent settlements, namely, no chance to exceed the "equivalent quake" of the pile in Boom clay.

The SKW results are also interesting because they authorize the comparison of two sets of tests performed on the same pile with a temporal gap of one year. The displacements remain in the same range for both maximal and permanent categories. There is no distinction between pile/soil system responses from both years.

The same data have been generated for the piles B8 and B9 in the Bruxellian sand of Limelette. The maximum values of both series are slightly different because the drop height schedule is different (until 2.6 m for pile B9 where it is only 2.0 m for pile B8).

	B8 - Limelette	B8 - Limelette	B9 - Limelette	B9 – Limelette
Blow No	**Max Setl. [m]**	**Perm Setl. [m]**	**Max Setl. [m]**	**Perm Setl. [m]**
1	3.3	0.4	3.5	0.2
2	5.4	0.5	5.3	0.2
3	6.2	0.4	5.4	0
4	6.5	0.4	6.3	0.4
5	7.1	0.1	7.3	0.7
6	5.9	0.3	5.4	0.2
7	7.7	0.4	8	0.7
8	6.8	0.4	8.3	0.3
9	8.7	0.1	8.5	0.5
10	6.1	0.5	6.8	0
11	9.4	0.9	11	0.7
12	7.9	0.7	6	0
13	9.5	0.8	10.1	1.9
14	11	2.5	8	1

15	11.9	3.9	11.3	3.5
16	11.8	4.4	9.6	2.6
17			9.8	2.2
18			12.5	5.2
19			14.8	6.6
20			14.9	7.1
Min	***3.3***	***0.1***	***3.5***	***0.2***
Max	***11.9***	***4.4***	***14.9***	***7.1***

Table III-6 : Maximum and permanent settlements during DLT for Limelette site

Figure III-33 shows the curves of displacement based on the measured signals of acceleration for the pile B8. The attenuation is less pronounced than for the tests in clays (more than 1 oscillation before stabilization of the signals). On the other hand, the permanent settlement does not increase with the drop height as faster as for the tests in clay. Figure III-34 confirms that the trends observed for the tests in clays are confirmed: evolution of the slopes and a constant settlement gap (the rebound) between both curves from a certain drop height called the critical height. But the height of drop required to have a significant permanent settlement increases to 1.3 – 1.5 m. Consequently, a major part of the tests performed in Limelette do not present significant permanent settlements.

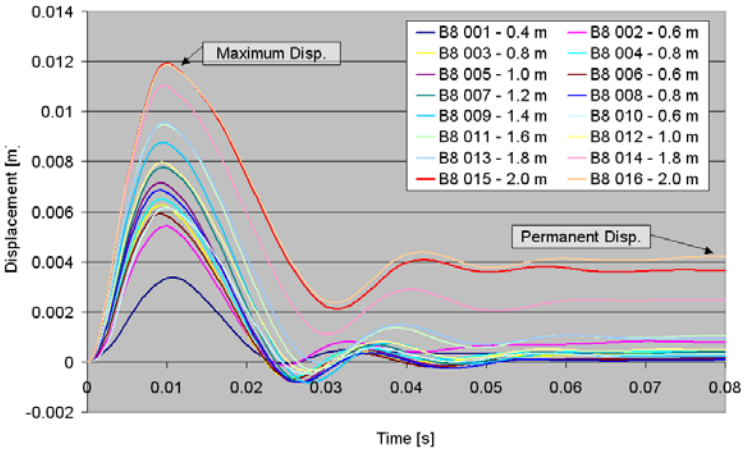

Figure III-33 : Plot of the displacement curves for the pile B8 of Limelette

Figure III-35 compares both results (drop height vs. max & perm settl.) from tests in clay and sand.

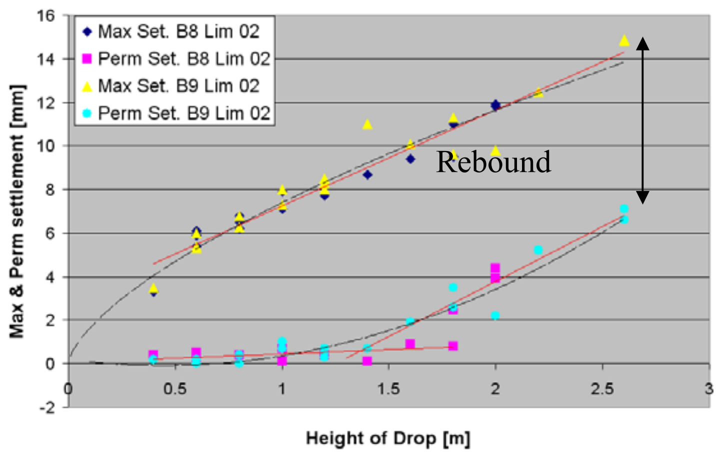

Figure III-34 : Heights of drop vs. maximum & permanent settlements (Piles B8-B9 - Lim)

The maximum settlement trends seems to be complementary since the Limelette's points look like following the SKW's points. On the other hand, the permanent settlements trends show typical behaviours for both types of soil. The critical height is higher for sand and their slope seems to be stiffer as well. This is characteristic of the soil type: the more resistant the soil, the higher the drop to cause a significant driving.

The height of drop is linked to the energy transmitted or the work done by the pile with regards to the efficiency rate of the hammer, ram or any machine providing the dynamic force on the pile head. However this efficiency is not known and can be variable, influencing the above analysis.

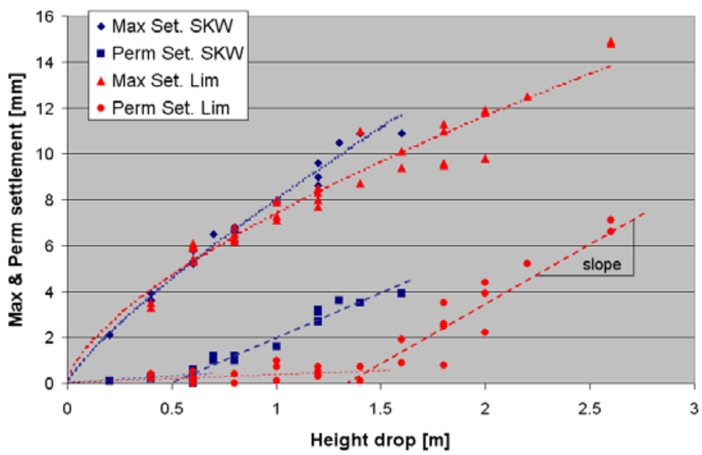

Figure III-35 : Heights of drop vs. maximum & permanent settlements (Sites SKW - Lim)

The following section approaches a more rational point of view. Instead of drop height in the previous figures, the maximum velocity of the pile head, the maximum force or energy transmitted to the pile are used vs. settlements.

Gossuin (2001) analysed the response of the pile/soil system to driving by using the program GRLWEAP© and simulating the equivalent of Figure III-32 for a variation of shaft and base resistances. He particularly studied the influence of these changes in the required height to produce a significant permanent settlement, on the rebound and on the slope of the permanent settlement trace. He concludes that the critical drop height needed to produce a permanent settlement is highly dependent of the ratio of shaft resistance in the total capacity: the higher the ratio and the lower the critical height. What is recovered in Figure III-35 where the critical height is inferior in the clayey site compared with the sandy site. He also concludes that the slope of the permanent settlement must decrease if both the total resistance and the ratio Q_{frot}/Q_{total} increase. This last conclusion is in opposition with the observations made herein since the total capacity in the sandy soil is superior to the corresponding one in clayed soil and the ratio Q_{frot}/Q_{total} is also inferior for sandy soil but the slope appears to be higher. However, it can be concluded that the observations made for the specific driving analysis can be used for the analysis of dynamic load test data.

3.3.2 Maximum velocities and dynamic settlements

Table III-7 provides the maximum velocities of the pile head for all tests investigated.

	A7 – SKW (99)	**A7 – SKW (00)**	**B8 - Limelette**	**B9 - Limelette**
Blow No	**Max Velocity [m/s]**	**Max Vel. [m/s]**	**Max Vel. [m/s]**	**Max Vel. [m/s]**
1	0.66	0.42	0.54	0.57
2	1.46	0.83	0.97	1
3	1.87	1.14	1.15	1.05
4	1.58	1.16	1.19	1.22
5	1.97	1.1	1.31	1.42
6	2.23	1.39	1.09	1.02
7	1.61	1.7	1.39	1.53
8		1.51	1.26	1.56

9		2.05	1.58	1.61
10		1.5	1.11	1.28
11		2.27	1.65	1.67
12		1.37	1.46	1.14
13		2.28	1.74	1.84
14			1.9	1.49
15			2	1.96
16			1.98	1.71
17				1.72
18				2.06
19				2.24
20				2.27
Min	***0.66***	***0.42***	***0.54***	***1.14***
Max	***2.23***	***2.28***	***1.98***	***2.27***

Table III-7 : Maximum velocities during DLT for both sites

Based on the results of Table III-4 and Table III-7, for a given drop height, the maximum velocity is superior in clay. However, even if the type of soil is of importance, the efficiency of the dropping system (manual dropping by the crane operator) is certainly also involved.

Figure III-36 shows the comparison of the maximum velocities vs. drop heights for both sites. Figure III-37 shows the curves of the velocities evaluated from the measured signals of acceleration of the pile A7 of Sint-Katelijne-Waver during the 1st set of tests (1999). The traces confirm the increase of the peak velocity with the drop height, the relative repeatability for same drop heights (even if the posterior tests performed at the same height of drop present a slight higher peak velocity) and the quick attenuation of the signal (over a period of 0.04 s).

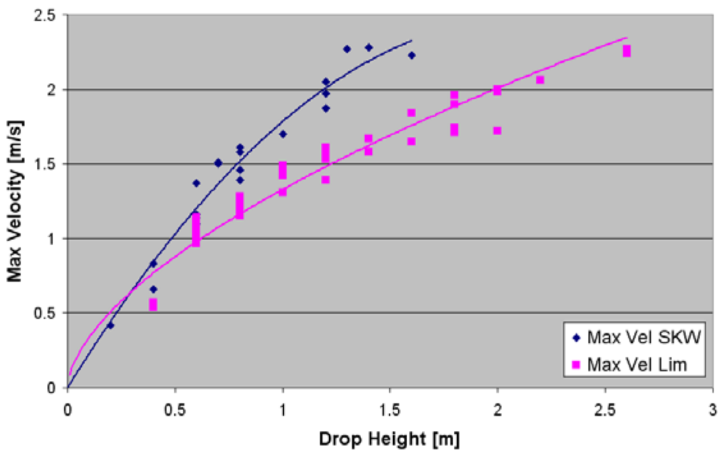

Figure III-36 : Height of Drop vs. maximum velocity (Sites SKW - Lim)

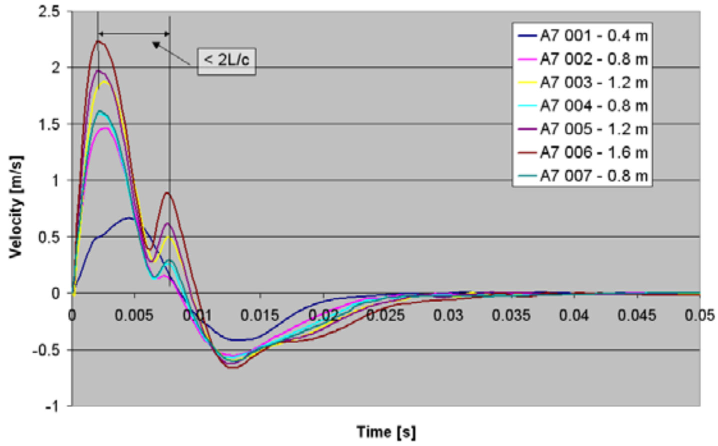

Figure III-37 : Plot of the velocity curves for A7 (99) of SKW

The curves show a second peak most probably connected to the return of the wave after reflection on the base. Figure III-38 exhibits the maximum and the permanent settlements vs. the maximum velocity of the pile head during the test for the clayed site of Sint-Katerijne Waver. The maximum velocities present a trend very well fitted with a straight line almost crossing the origin but this behaviour can also be fitted with a set of two consecutive straight lines (the first, from the origin, and the second, stiffer, when the permanent settlements start to be generated).

Moreover, the permanent settlement indicates clearly two pronounced behaviours marked by the velocity 1.2 – 1.3 m/s (critical velocity?).

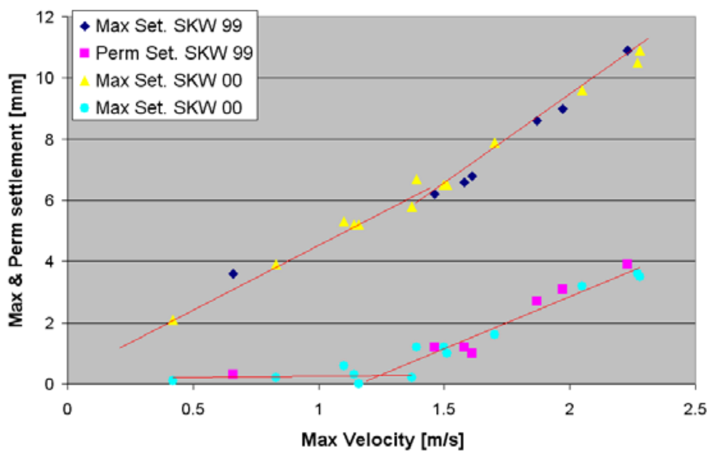

Figure III-38 : Maximum velocity vs. maximum & permanent settlements (Pile A7 (99 & 00) - SKW)

As for Figure III-37, Figure III-39 presents the traces of velocity measured on the pile B8 in sand. The signals corresponding to a same drop height evolves with the chedule of drop height: the traces are amplified maybe denoting a certain degradation of the soil response (a smaller resistance along the pile shaft and a highr velocity) due to the loading history.

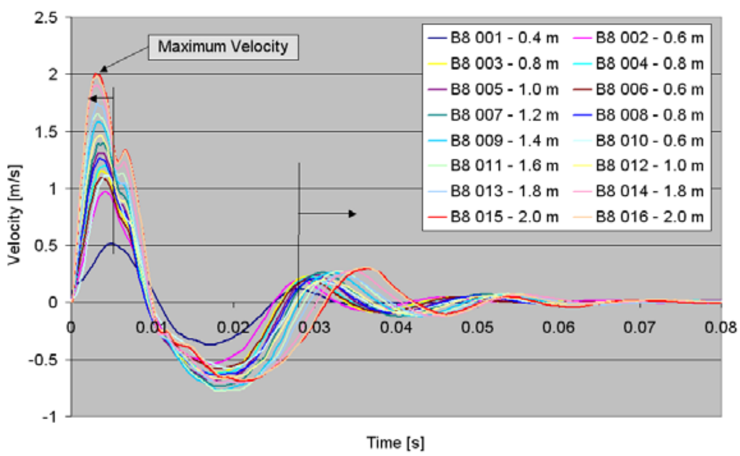

Figure III-39 : Plot of the velocity curves for the pile B8 of Limelette

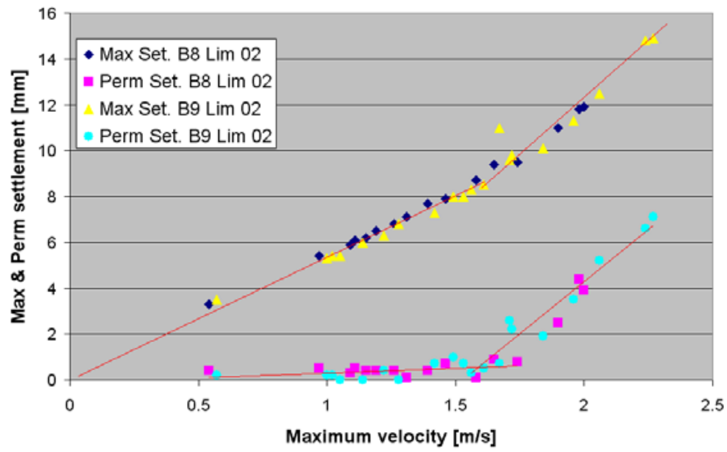

<u>Figure III-40</u> : Maximum velocity vs. maximum & permanent settlements (Piles B8-B9 - Lim)

The signals attenuate slowly compared to the clayed site: the signals seem to be stabilized for only t = 0.08 s. Globally, the frequency of the damped sinus evolves (decreases) when the drop height and the peak velocity increases. The first peak of velocity arrives more rapidly if the velocity is high and the second velocity peak "recedes". <u>Figure III-40</u> is the mirror of <u>Figure III-38</u> for the tests performed in sand. The trend of the maximum settlement is also almost linear with velocity but an increase of slope in the range of high velocities indicates a modification of behaviour when significant permanent settlements start to be generated. The permanent settlement traces show two distinct behaviours marked for a maximum velocity of ~ 1.6 m/s. There is no difference between the results of piles B8 and B9. The trend is similar.

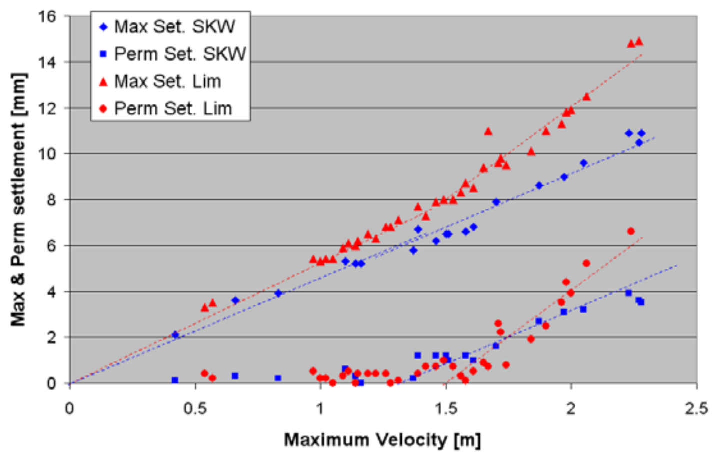

<u>Figure III-41</u> : Maximum velocity vs. maximum & permanent settlements (Sites SKW - Lim)

<u>Figure III-41</u> gathers <u>Figure III-38</u> and <u>Figure III-40</u>. Both classes of settlement (perm and max) present a linear relationship of the max velocities in both soil types. It is also shown that the ratio of settlement by unit of velocity is higher for sand than for clay.

Finally, a link can be done between the drop height (linked to the potential energy) and the maximum velocity measured (linked to the kinetic energy). The velocity of the pile head can be expressed, theoretically and for an infinite pile, to the ratio of ram and pile impedances and to the impact velocity (Holeyman, 1984). This impact velocity is itself linked to the drop height by the kinetic energy and the efficiency of the impact system. If this efficiency is noted η_i, the drop height is linked to the maximum velocity by:

$$\sqrt{2g \cdot h} \cdot \eta_i = v_i = f(v) \qquad \textbf{Equ. III- 35}$$

Where v_i is the impact velocity.

The plot of $\sqrt{2g \cdot h}$ vs. the measured maximum velocity gives:

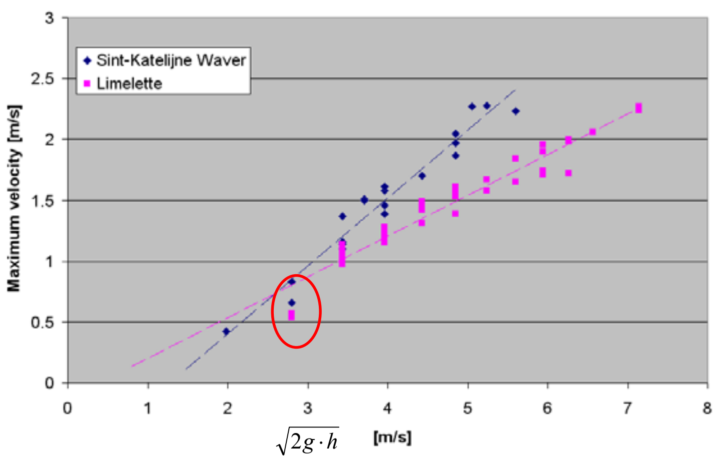

<u>Figure III-42</u> : Relationship between the maximum velocity measured and the drop height

The trend is linear for both sites but the regression straight line does not cross the X axis at the origin for the clayed site. This may be due to the fact that in clay, when the velocity reaches its maximum, the effects of the first layers of clay could have already influenced the velocity by reducing it (upwards waves and reduction of the measured velocity). The sand shows a similar trend for the first two points (corresponding to the first blows on both piles B8-B9) where the velocity is inferior to the expected result given by the regression line. At this moment, the first layers still influence the total resistance, but after, this effect vanished and is degraded and the maximum velocity remains not influenced by the friction upward waves of the first layers of soil.

3.3.3 Force and energy

Contrarily to the settlement (maximum and permanent) and the maximum velocity used previously that are both based on the acceleration signal, the force is coming from the second signal measured on site: the strain. This signal is less reliable than acceleration because of its sensitivity to the eccentricity of the impact on the pile head and also due to the higher variability of the parameters required to transform the strain into force compared to the integration procedure of the acceleration. All these developments will be presented with more details on the section focused on the quality of the signal, but it is important to introduce this point here because of the bad quality of 8 of 13 signals of the second phase of tests of the pile A7 of Sint-Katelijne-Waver. The signals of the drops #6 → #13 are consequently not presented in the force and energy analysis. The details of this malfunction are presented in the quality section. This section is focused on the force and energy (or Enthru) signal s analysis.

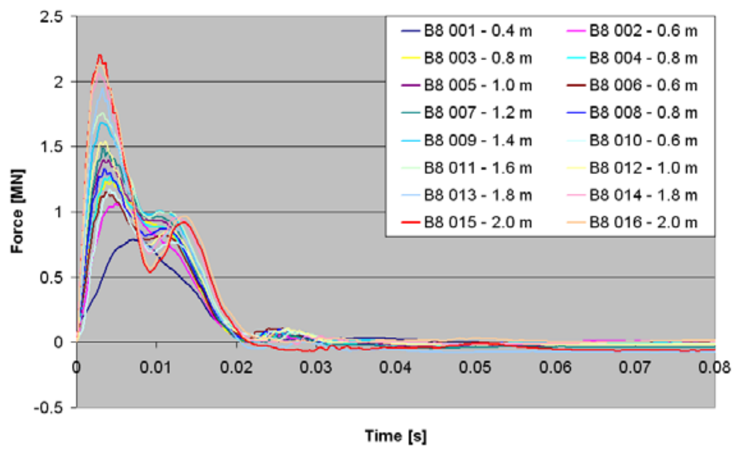

Figure III-43 : Plot of the force curves for the pile B8 of Limelette

Figure III-43 presents the traces of the force measured at the pile head for the pile B8 of the site of Limelette. The figures of the site of SKW are comparable but higher in magnitude and shorter in duration (width of the force pulse). Table III-8 summarizes the maximum values for both sites. Both maximum and minimum specific values are superior for the clayed site. This is due to the stronger load rate effects in clay compared to the sand response. The force traces are (almost) always positive or null. That confirms that the pile does not undergo traction during the test. The small negative values are the result of to the averaging of the measurements from the two transducers (and including the eccentricity effects).

	A7 – SKW (99)	**A7 – SKW (00)**	**B8 - Limelette**	**B9 – Limelette**
Blow No	**Max Force [MN]**	**Max Force [MN]**	**Max Force [MN]**	**Max Force [MN]**
1	1.576	1.039	0.787	0.833
2	2.264	1.571	1.061	1.138
3	2.751	1.933	1.237	1.154
4	2.344	1.863	1.274	1.358
5	2.794	1.897	1.400	1.537
6	3.112	Not Valid	1.157	1.116
7	2.358	Not Valid	1.492	1.670
8		Not Valid	1.329	1.725
9		Not Valid	1.687	1.787
10		Not Valid	1.173	1.415
11		Not Valid	1.762	1.823
12		Not Valid	1.541	1.248
13		Not Valid	1.950	2.025
14			2.062	1.632
15			2.207	2.164
16			2.132	1.874
17				1.883
18				2.236
19				2.450
20				2.659
Min	***1.576***	***1.039***	***0.787***	***0.833***
Max	***3.112***	***1.933***	***2.207***	***2.659***

Table III-8 : Maximum forces measured during DLT for both sites

Figure III-44 presents the comparison of the maximum measured force vs. the maximum and permanent settlements. Similar observations than for the velocity analysis can be made: the driving behaviour is conditioned in two "linear" phases. The first phase is characterized by an absence of final settlement until reaching a certain level of force. This value is fixed to 1900 to 2000 KN for clay and 1700 to 1800 KN for sand.

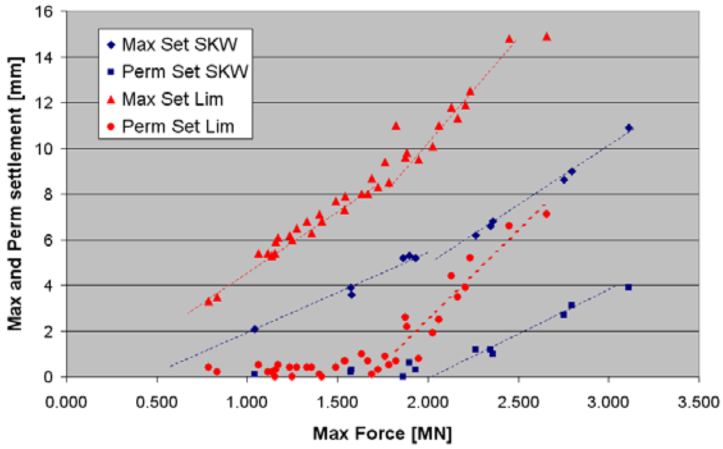

<u>Figure III-44</u> : Maximum force vs. maximum & permanent settlements (Sites SKW - Lim)

The behaviour of the maximum settlement regarding to the force seems to be also influenced by this particular value, changing the slope of the regression straight line. Once the permanent settlement reaches not-null values, the evolution of both settlements (perm and max) is nearly parallel but stiffer for sand than for clay.

When the maximum force is compared to the maximum measured velocity, the trend observed must reflect the nominal impedance of the pile (wave equation section in chapter 1).

<u>Figure III-45</u> shows the plot of these points for both sites and parallel trends are highlighted by the linear regression (in black). The dashed red line corresponds to the slope of the nominal impedance and is nearly perfectly parallel to the lines based on measurements. However, the data of the clayey site exhibit a linear relationship that does not reach the origin. The explanation can be the same that for <u>Figure III-42</u>: the velocity signal is reduced by the upward waves, and on the other hand, the force is also modified in the opposite way (increase of force due to the upwards waves), both effects brings out a permanent gap.

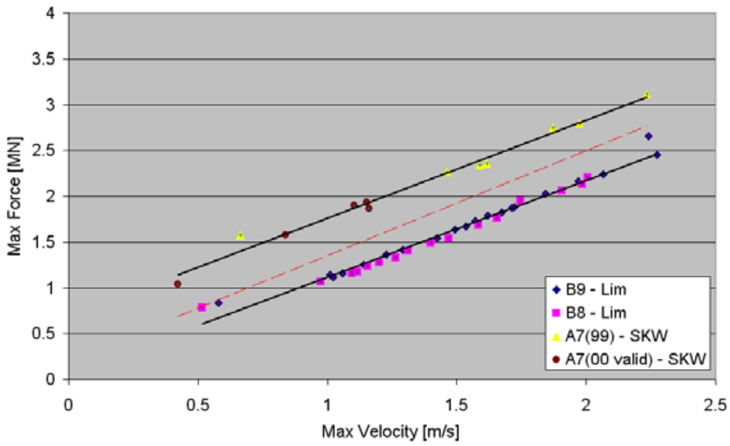

<u>Figure III-45</u> : Max force vs. max velocity (SKW - Lim)

The energy transmitted to the pile is called “Enthru”. It is defined as the integration of the product of both force and velocity signals until the end of impact (t_f)

$$Enthru = \int_0^{t_f} F(t) \cdot v(t) \cdot dt$$ **Equ. III- 36**

Figure III-46 shows the traces of Enthru for the pile B8 of Limelette. As expected, the transferred energy increases with the height of drop.

The value taken into account is the maximum peak value corresponding to the integration of the positive pulse of velocity without considering the negative part of the velocity. Table III-9 summarizes the results of the maximum enthru calculated for both sites.

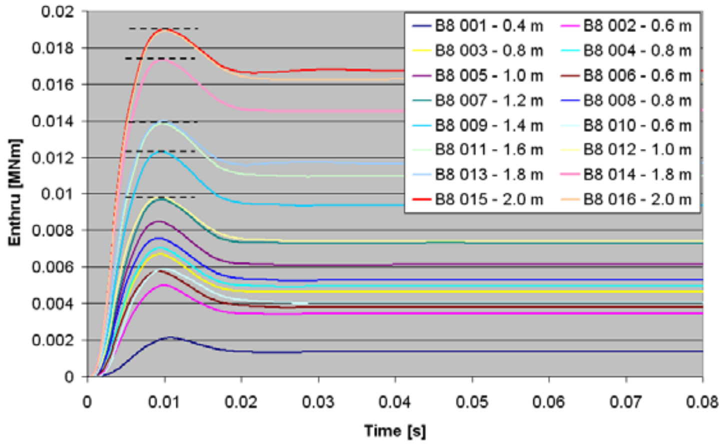

Figure III-46 : Plot of the energy transferred curves for the pile B8 of Limelette

	A7 – SKW (99)	A7 – SKW (00)	B8 – Limelette	B9 - Limelette
Blow No	**Enthru [MNm]**	**Enthru [MNm]**	**Enthru [MNm]**	**Enthru [MNm]**
1	0.004387	0.001634	0.002122	0.002336
2	0.012107	0.004907	0.004995	0.005185
3	0.019608	0.008370	0.006698	0.005286
4	0.013299	0.008270	0.007035	0.00721
5	0.020539	0.008147	0.008492	0.009536
6	0.026425	Not valid	0.00575	0.00502
7	0.013638	Not valid	0.009692	0.011064
8		Not valid	0.007566	0.011844
9		Not valid	0.012320	0.012296
10		Not valid	0.005879	0.007937
11		Not valid	0.013855	0.013307
12		Not valid	0.009827	0.006207
13		Not valid	0.013991	0.016149
14			0.017376	0.010663
15			0.019025	0.018445
16			0.018919	0.014176
17				0.014405
18				0.02072
19				0.027035
20				0.028390
Min	***0.004387***	***0.001634***	***0.002122***	***0.002336***
Max	***0.026425***	***0.00837***	***0.019025***	***0.02839***

Table III-9 : Maximum enthru during DLT for both sites

Figure III-47 presents the comparison of the Enthru and the permanent and maximum settlements. The same observations than previously are still valid. The trend curves are not linear but are similar to the drop height analysis (section 3.3.1). The instant slope of the maximum curve decreases from origin to almost stabilize. The energy values of slippage starting are 0.008 to 0.01 MNm for clay and 0.012 MNm for sand.

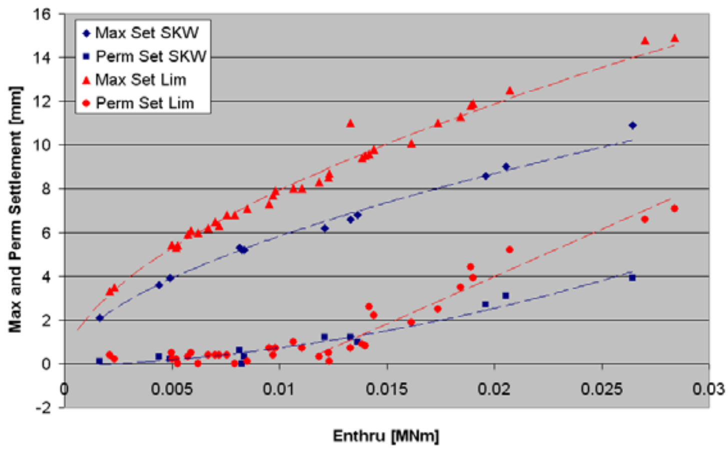

Figure III-47 : Maximum enthru vs. maximum & permanent settlements (Sites SKW - Lim)

The comparison of the Enthru with the potential energy (Figure III-48) illustrates the efficiency of the testing system. The data are arranged linearly for both sites. The dashed lines correspond to the data regression of each sites. The efficiency is the ratio of the Enthru by the potential energy (slope of the dashed lines). The efficiency in Sint-Katelijne-Waver is 48 % and the ratio in Limelette is equal to 27 %.

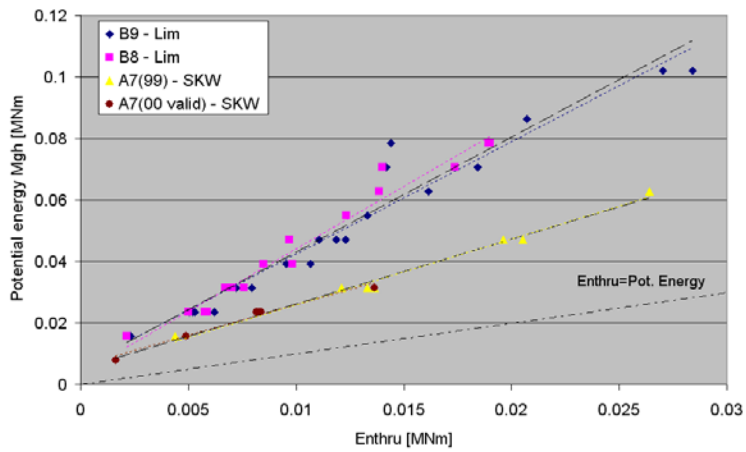

Figure III-48 : Maximum enthru vs. theoretical potential energy (Sites SWK - Lim)

3.4. Visualisation of the dynamic motion signal along the pile

The dynamic testing of pile is characterised by the wave propagation effect into the pile. It can give a tomography of the pile in depth if the reception of the wave in time at the pile head is analysed with this purpose (see chapter 1, section 3.2.3.3.). This phenomenon is rendered by the spring mass system supposed to model the axial pile behaviour under axial solicitation. Considering this model and considering a real signal injected at the head (for example the velocity signal). The visualization of the motion of all pile elements vs. time may represent the wave propagation.

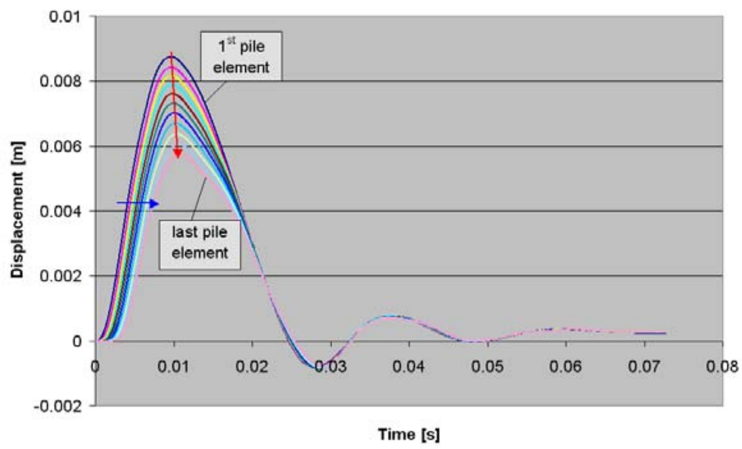

<u>Figure III-49</u> : Pile elements displacement during a dynamic load test

The displacement figure is very explicit. The wave propagation (blue arrow) is coupled with the load transfer generating a differential shortening of each pile element. After a period of about 20 ms, all the pile elements are synchronised and the pile moves as a rigid body due to the wave propagation into the pile. The red arrow gives an information about the load transmitted to the pile base: the reduction in displacement between the maxima is due to the elastic shortening of the elements and to the dynamic load transmitted to shaft and base, respectively.

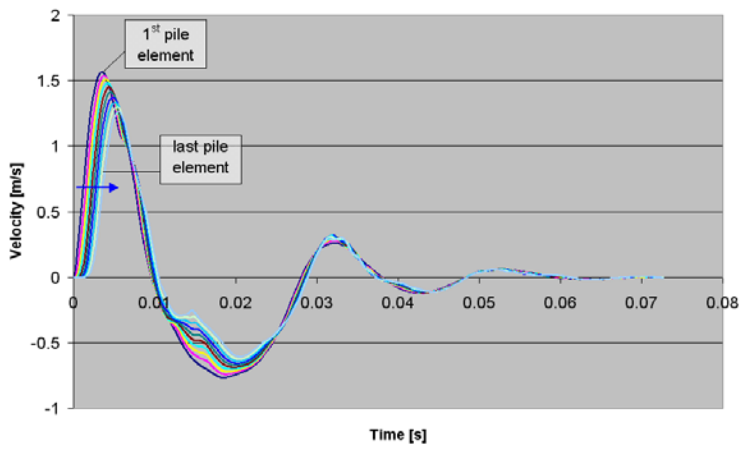

<u>Figure III-50</u> : Pile element velocity during a dynamic load test

The velocity figure shows the same situation. The velocity traces evolve together after the same duration of about 20 ms like in <u>Figure III-49</u>. The main trend of each element's trace illustrates the general behaviour of the pile and is coming from the input signal at the pile top (blue trace in detail (a)-<u>Figure III-51</u>). Consequently, the information "goes down" the pile with the wave propagation. Sometimes the information can come from the bas reaction due to a particular reflection and the information goes up to the top (grey trace in detail (b)-<u>Figure III-51</u>).

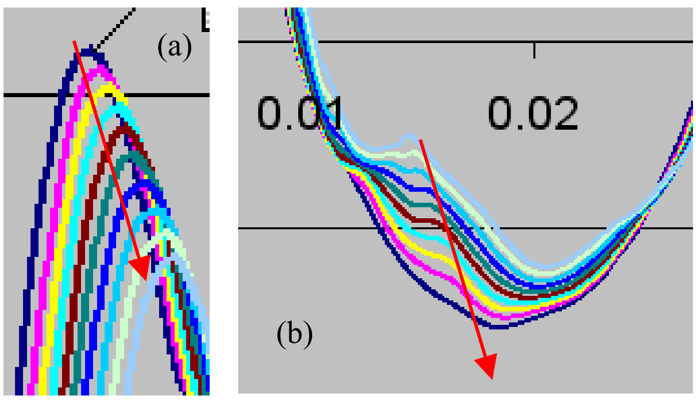

<u>Figure III-51</u> : Propagation of the information from the top (a) or from the base (b)

3.5. Signal quality check

The signal quality check is an essential part of the process of analysis of the dynamic data. This analysis needs fair data representative of the measured behaviour. This obvious remark requires hypothesis, verifications and good evaluations of certain quantities.

First, the data must be correctly measured and the blow must be correctly given to the pile head. To ensure this fact, several operations can be done:

- On field, the observation of the complete progress of the test is needful, including the control of the alignment of the mass and the pile axis, the correct fixation of the transducers, the verification of the data acquisition chain and the verification of the height and the free fall behaviour of the dropping system;
- The strain and the acceleration are both measured on two independent channels placed diametrically opposite on the pile shaft. Their comparison allows to check the potential eccentricity of the blow;
- The data of acceleration and strain are measured with respect to time. The storage starts before the blow and ends after stabilization of the pile. Consequently, both acceleration and strain values have to be equal to zero at the start and at the end of each blow.

After, the acceleration and the strain are transformed in velocity and displacement, and in force respectively. These operations also need hypothesis.

3.5.1 The field measurements

A. <u>The acceleration</u> is measured with accelerometers (2) generally fixed on the pile shaft. <u>Figure III-52</u> presents the traces of both measured signals and the average one used in the analysis. The following remarks can be pointed out in parallel with the marks on the figure.

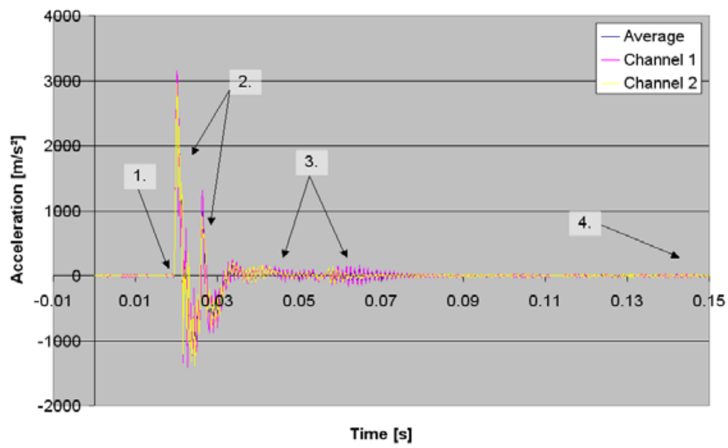

<u>Figure III-52</u> : Acceleration measurements (2 channels + average)

1. The impact: both signals start at the same time with the same slope. Good synchronisation;

2. When the blow has just impacted the pile head, the accelerations are also in phase;

3. After the main part of the signal, the pile starts to vibrate. The opposition of phases indicates that it is probably a parasite vibration due to a slight eccentricity in the horizontal plan. The averaging corrects this influence but can generate spurious velocity;

4. The end of signal, the acceleration has to be equal to zero in order to generate correct velocity and displacement after integration.

This average signal renders correctly the single ones as it is generally the case for acceleration. This kind of signal is very stable to eccentricity.

B. The strain is measured with strain gages fixed on the pile shaft 2 or 3 diameters below the pile head to avoid the local stress generated by the geometrical particularities.

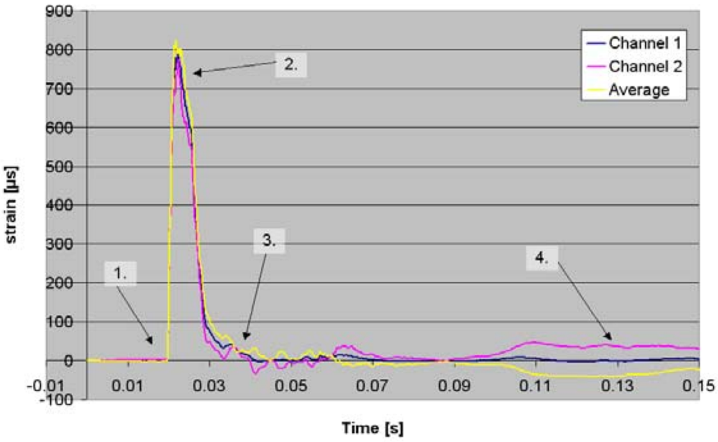

Figure III-53 : Strain measurements (2 channels + average)

Figure III-53 shows the stress measurements from both transducers. The graph plots the single traces and their average used in the analysis. The following remarks can be given:

1. Synchronization of the signals at the start;

2. The major part of the signal is similar for the three traces;

3. The end of the energetic part shows a differentiation that corresponds with the vibrations appeared in the acceleration figure (Figure III-52). The pile vibrates around its vertical axis and generate slight tensions. A slight eccentricity is brought out;

4. The end of the signal exhibit opposed behaviours averaged with a expected null value. That corresponds probably to the blow eccentricity or the pile horizontal vibrations.

The strain signal is more sensitive to the eccentricity than the acceleration. Generally, the average trace of both signals is considered as the correction to this eccentricity. This is true for a small difference such as the difference seen in Figure III-53. But if the eccentricity becomes pronounced or located in another vertical plane than the plane defined by both transducers, the average can introduce errors that generally over or under-estimate the force signal. The data withdrawn from the analysis in section 3.3.3 of this chapter were improper because of the effect of eccentricity to the force measurements:

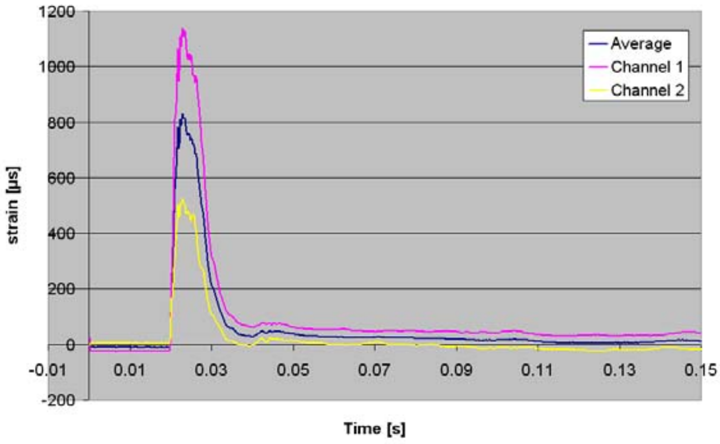

Figure III-54 : Bad strain measurements (2 channels + average)

Figure III-54 shows the effect of a strong eccentricity: a large deviation between both stress measurements, and a large uncertainty on the average data measured. The origin of this eccentricity can be variable: e.g. a misalignment of the ram with the pile axis or the failure of the pile causing a differential settlement. The consequences can lead to a bad interpretation of the signals. The consequences on the relationships between the measured force and the Enthru (Figure III-45 to Figure III-48) are obvious and illustrated here below.

Figure III-55 and Figure III-56 express clearly that the forces measurements are badly influenced. The dashed red arrows indicate the large consequence if only one signal of force is used instead of the average trace. The force chosen is the smallest one and is probably under-estimated in comparison with the real one. The "corrected" value should reach the trend of the old A7 results.

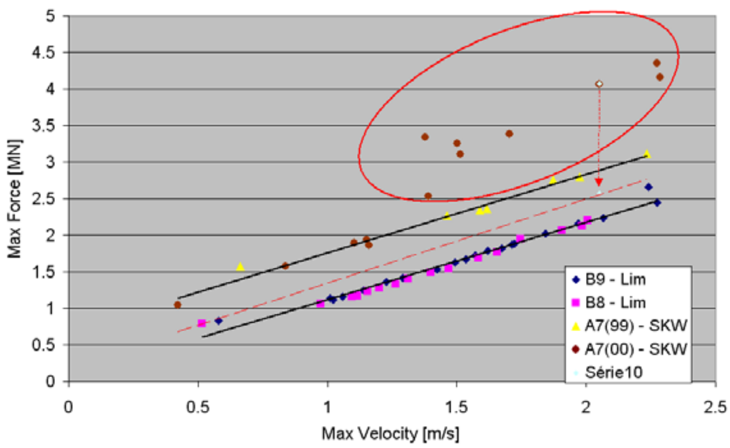

Figure III-55 : Addition of questionable data to Figure III-65 to highlight the effects of large eccentricity on the quality of data

It is also shown on Figure III-54 that the initial and the final values of the strain measurements are not equal to zero what is a serious indication of the quality of the measurements.

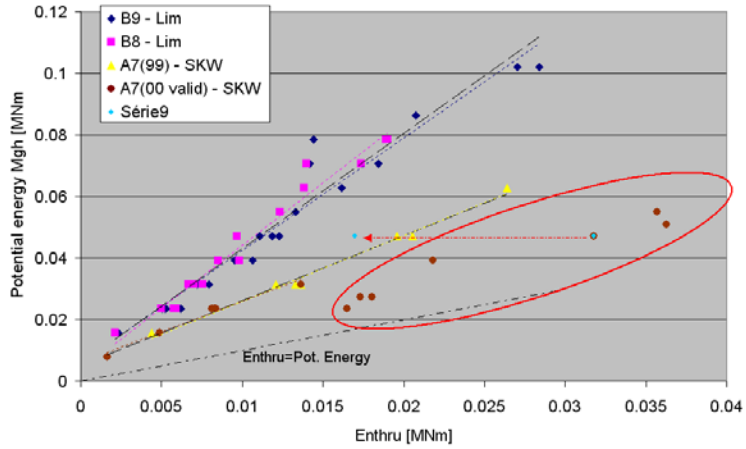

Figure III-56 : Addition of wrong data to Figure III-68 to highlight the effects of large eccentricity on the quality of data

3.5.2 The post-treatment

If the measurements are estimated reliable, the post-treatment needs also to be correctly performed because of the assessment required for this post-treatment.

3.5.2.1 From strain to force

The force is linked to the strain by the Hooke's law:

$$F = A \cdot E \cdot \varepsilon$$ **Equ. III- 37**

- A is the pile normal section [m²];
- ε is the strain [-];

and E the elastic modulus is given by: $E = v_p^2 \cdot \rho$ **Equ. III- 38**

- v_p is the wave velocity [m/s];
- ρ is the mass density of the pile material [kg/m³]

Compared to the pile head velocity that is almost directly measured, the force signal depends on the pile section and especially on the wave propagation velocity. However, the latter parameter is more variable[3] than the mass density and the pile section. The wave propagation is directly connected to the concrete strength that depends on the type of cement and on the age of concrete after casting.

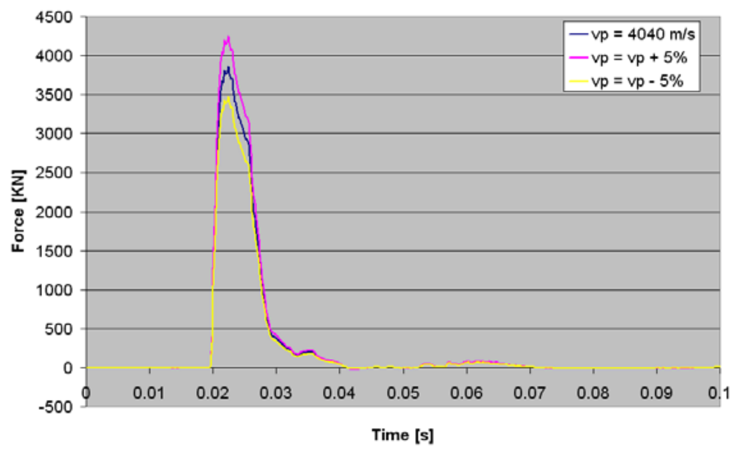

Figure III-57 : Influence of v_p on the force precision

Figure III-57 presents the influence

[3] For concrete

of the modification of 5% (fewer or extra) of the wave propagation velocity on the force evaluated. Since the force is used directly as input or reference in the back-analysis process, the importance of this step is highlighted. But possibilities exist to evaluate the wave propagation velocity:

- Laboratory methods (empirical relationships);
- Ultrasonic method (wave auscultation);
- Analyse of the signals measured.

The last method uses two properties of the wave equation analysis applied to piles:

- as already explained (chapter 1 and section 3.2.3.3.) the force and the velocity are proportional with respect to the pile nominal impedance (I) during the first instants of the blow when the upwards waves of the first shaft layers do not perturb the measurements yet:

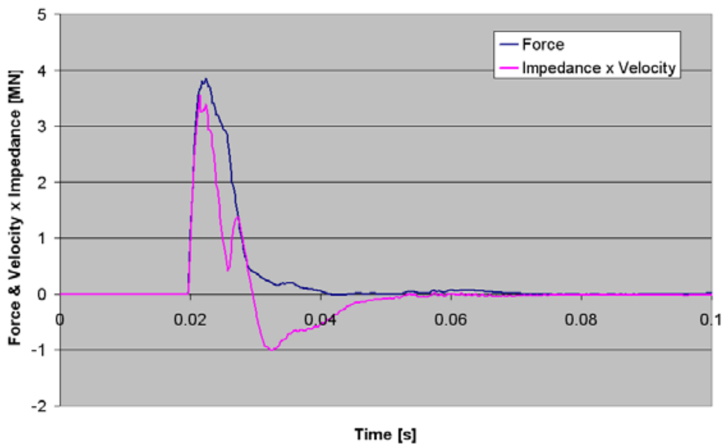

<u>Figure III-58</u> : Relationship between force and velocity x impedance

$$F = VI \text{ and } I = \rho \cdot v_p \cdot A \qquad \textbf{Equ. III- 39}$$

In the case of a pile where this duration is sufficiently long, a matching procedure of both signals in order to best fit the first part of them can inform for the value of v_p (<u>Figure III-58</u>).

- Another method is to analyse the upwards waves given by:

When the upwards wave presents a local peak, it corresponds to the end return of the information reflecting to the base. This return may be characterized by the time needed to travel 2 pile lengths. This time is equal to $2L/v_p$ giving an information on the value of the propagation velocity v_p (<u>Figure III-59</u>).

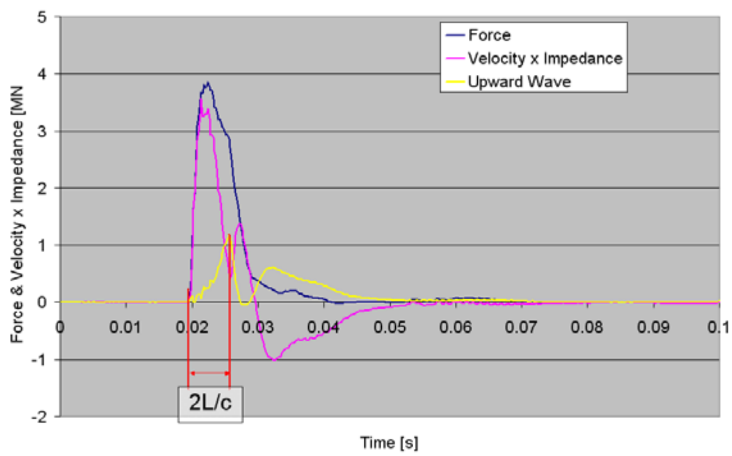

<u>Figure III-59</u> : Use of the upwards wave to evaluate the wave propagation velocity

$$F \uparrow = \frac{1}{2}(F - VI)$$ **Equ. III- 40**

3.5.2.2 From acceleration to velocity and displacement

The acceleration is integrated with respect to time to evaluate the velocity and the displacement. However, the integration procedure can be perturbed by the miss of the constants of integration during those two processes. This correction is taken into account by the possibility to equal the permanent settlement to a fixed value. This operation is visual and allows to correct the kinetic data.

4. Conclusions

Mainly based on the pile/soil model, the first part of this chapter describes the distinct shaft and base soil reactions by defining the specific terms linked to the small and large deformations and the static and dynamic solicitations. Afterwards, a special attention is put on the classification of the parameters in order to reduce their number before the optimization process. Finally, a parametric study of two dynamic parameters (the main frequency and the magnitude of the dynamic solicitation) allowed to described the influence of each term involved in the load rate effect at different steps of the load-displacement curve (initial stiffness, failure, …). It appears that, in the range of the dynamic solicitations, the radiation damping influences greatly the magnitude and the initial stiffness of the dynamic soil reaction compared to the viscous term.

The second part of this chapter is mainly focused on the measurements made during a dynamic load test. The date used in this research come from a national research program organized by the BBRI which is shortly described. Afterwards, a specific analysis is carried out upon the measurements. This strict analysis is based on the reached maxima of quantities such as displacement or settlement (perm or max), velocity, force or transferred energy on the top of the pile that bring similar results between couple of quantities. Figure III-32, Figure III-34, Figure III-38, Figure III-40, Figure III-44 and Figure III-47 illustrate with the same accuracy that there is a need for a minimal drop height, velocity and force of energy to develop a substantial permanent settlement. This settlement develops later quasi in parallel with the evolution of the maximum reached settlement. Depending on the quantity used, the curves present two types of behaviours. The maximum settlement curve presents a convex evolution in function of height of drop or the Enthru. On the other hand, the maximum settlement curve presents a concave[4] evolution in function of the velocity or the maximum force. A summary of the required quantities to develop a significant permanent settlement is given by:

	Sint-Katelijne-Waver	Limelette
Drop Height [m]	0.5 – 0.7	1.3 – 1.4
Maximum Velocity [m/s]	1.2 – 1.4	1.5 – 1.6
Maximum Force [MN]	1.9 – 2.0	1.75 – 1.8
Energy [MNm]	0.007	0.012 – 0.03

Table III-10: Summary of the critical quantities to get significant permanent settlement

[4] Or a sum of two straight lines with the stiffer in second position.

The analysis of the measurements has also highlighted theoretical results expected between measured quantities. For example the relationships between force and velocity measured at the pile head or energy transmitted and the drop height (translated in potential energy).

Another good result is the repeatability of same tests performed on a pile. Despite the fact that a slight trend to degradation of resistance is observed when several blows of same height drop were compared (especially in Limelette), in general the same response is measured after submission to a similar solicitation. Moreover, in each site, an internal comparison allows the comparison of the effects of the pile resting in the soil during one complete year for Sint-Katelijne-Waver and the comparison of the behaviour of two identical piles installed in the same soil and tested similarly in the same day for Limelette. The results bring no clear distinct trends for both particular comparisons what is remarkable and allows conclusions to be given only for soils and sites.